



BRNO UNIVERSITY OF TECHNOLOGY

VYSOKÉ UČENÍ TECHNICKÉ V BRNĚ

FACULTY OF MECHANICAL ENGINEERING

FAKULTA STROJNÍHO INŽENÝRSTVÍ

INSTITUTE OF AEROSPACE ENGINEERING

LETECKÝ ÚSTAV

SMALL SATELLITE DISPENSER STRUCTURAL OPTIMIZATION

OPTIMALIZACE NOSIČE SATELITŮ

MASTER'S THESIS

DIPLOMOVÁ PRÁCE

AUTHOR

AUTOR PRÁCE

Bc. Jakub Zíka

SUPERVISOR

VEDOUCÍ PRÁCE

Ing. Robert Popela, Ph.D.

BRNO 2020

Specification Master's Thesis

Department: Institute of Aerospace Engineering
Student: **Bc. Jakub Zíka**
Study programme: Mechanical Engineering
Study branch: Aircraft Design
Supervisor: **Ing. Robert Popela, Ph.D.**
Academic year: 2019/20

Pursuant to Act no. 111/1998 concerning universities and the BUT study and examination rules, you have been assigned the following topic by the institute director Master's Thesis:

Small satellite dispenser structural optimization

Concise characteristic of the task:

In the frame of SMSS "Small Satellites Mission Services" project there was designed small satellites dispenser for VEGA–C launcher. Dispenser is intended for multiple modular size satellites transport to low earth orbit. For current dispenser design there is necessary to analyze in detail eigenfrequencies and to optimize design to reach their acceptable values. Redesign shall not negatively affect weight of dispenser structure.

Goals Master's Thesis:

Creation of FEM computational model for structural and modal analyses of dispenser structure. Optimization of structure design for eigenfrequency limits compliance of dispenser. Minimization of weight penalty caused by any changes. Analysis of manufacturability.

Recommended bibliography:

MACDONALD, M.; International Handbook of Space Technology, Springer, 2014, ISBN-13: 978-3642411007.

MAINI, A. K., AGRAWAL, V.; Satellite Technology: Principles and Applications, Wiley, 2014, ISBN-13: 978-1118636473.

European Cooperation for Space Standardization (ECSS) documents, <https://ecss.nl/>

VEGA-C User's Manual, www.arianespace.com

Deadline for submission Master's Thesis is given by the Schedule of the Academic year 2019/20

In Brno,

L. S.

doc. Ing. Jaroslav Juračka, Ph.D.
Director of the Institute

doc. Ing. Jaroslav Katolický, Ph.D.
FME dean

ABSTRACT

This thesis is focused on stiffness optimization of small satellite carrying structure - the Dispenser. The first chapter is an introduction to the European space activities and also includes a brief technical overview of the European launchers. The second chapter aims to provide the finite element model description, which is used for the optimization, described in more detail in the third chapter. The fourth chapter concludes the thesis with the basic strength verification of the optimized structure.

KEYWORDS

small satellites Dispenser, optimization, finite element method

ABSTRAKT

Diplomová práce se zabývá tuhostní optimalizací nosiče satelitů, tzv. Dispenseru. První kapitola uvádí přehled evropských vesmírných aktivit a poskytuje nezbytné technické pozadí týkající se nosných raket. Druhá kapitola se věnuje popisu tvorby výpočetního modelu, neboť veškeré výpočty, včetně optimalizace popsané v kapitole třetí, jsou založeny na metodě konečných prvků. Pro optimalizovanou variantu je ve čtvrté kapitole provedena základní pevnostní kontrola.

KLÍČOVÁ SLOVA

nosič satelitů, optimalizace, metoda konečných prvků

ZÍKA, Jakub. *Small satellite dispenser structural optimization*. Brno, 2020, 78 p. Master's Thesis. Brno University of Technology, Faculty of Mechanical Engineering, Institute of Aerospace Engineering. Advised by Ing. Robert Popela, Ph.D.

ROZŠÍŘENÝ ABSTRAKT

Žijeme v moderní době, ve které jsou satelitní technologie naprosto běžnou součástí našich každodenních životů. S vývojem vědy a techniky a snahou o to vyrábět věci ve stále kompaktnějších rozměrech je dnes možné postavit umělou družici o velikosti Rubikovy kostky, vypustit ji na oběžnou dráhu a provádět s ní dálkový průzkum Země. V tomto ohledu začíná být nízká oběžná dráha Země oblíbenou destinací menších institucí (např. univerzit) pro účely plnění různých vědeckých misí.

Problémem však stále zůstává otázka vynášení těchto satelitů do vesmíru. Kvůli značné technické náročnosti vývoje a provozu nosných raket je transport nákladu do vesmíru extrémně drahou záležitostí. Tato skutečnost je ale převážně dána tím, že doposud byly rakety navrhovány tak, aby byly schopny vynést na oběžnou dráhu jeden až dva velké satelity. Se zmíněnými trendy zmenšování rozměrů satelitů je tedy nanejvýš výhodné přijít s technickým řešením, které umožní raketě vynést větší množství nákladu na oběžnou dráhu a tím pádem rozdělit cenu za start mezi více zákazníků. Tímto způsobem si let na raketě budou z hlediska financí moci dovolit i zmíněné malé instituce či firmy.

Vývoj takového nosiče satelitů s sebou přináší nespočet výzev. Každá raketa má svoji specifickou nosnost a přirozeným požadavkem každého zákazníka je přidělit co nejvíce této nosnosti hmotě jeho satelitu. Pokud raketa má do vesmíru nést satelitů více, musí být tyto satelity umístěny na podpůrné konstrukci, která logicky nosnost rakety snižuje, neboť sama o sobě žádnému jinému účelu nežli k uchycení satelitů neslouží. Cílem je tedy navrhnout velmi lehký nosič, který však musí vydržet extrémní zatížení, která vznikají při startu rakety. Krom nepřeberného množství jiných faktorů jsou při startu rakety obecně problémem vibrace. Vlastní frekvence takového nosiče satelitů musí na požadavek provozovatele rakety splňovat jisté limity, aby nedošlo při startu k nebezpečné rezonanci mezi raketou a nákladem a potenciální havárii.

Tato diplomová práce vznikla v úzké spolupráci s firmou SAB Aerospace, která se vývojem takového nosiče satelitů (tzv. Dispenseru) zabývá. Dispenser je určen pro evropskou lehkou nosnou raketu Vega a její silnější nástupkyni Vega-C. Během návrhu jedné z verzí tohoto nosiče se ukázalo, že konstrukce disponuje nižšími hodnotami vlastních frekvencí, než je pro bezpečný start povolené. Proto je cílem této práce celou konstrukci z hlediska tuhosti optimalizovat tak, aby se její vlastní frekvence dostaly do přípustných hodnot. Z předchozích úvah o nosnosti raket zároveň vyplývá, že optimalizovat konstrukci v tomto případě znamená dosáhnout požadovaných frekvencí při minimálním nárůstu hmotnosti.

Výpočetní problémy se v dnešní době téměř výhradně řeší numerickými metodami, v případě strukturální analýzy metodou konečných prvků. Jelikož Dispenser

společně s jeho nákladem několika desítek malých satelitů je velice komplexní struktura, celá jedna kapitola práce je věnována způsobům modelování a nastavování výpočetního modelu. Výpočetní modelování je v inženýrské praxi nástroj velmi mocný, nicméně je třeba k němu přistupovat kriticky a být si vědom všech kroků, zjednodušení a potenciálních chyb, kterých se při tvorbě modelů dopouštíme.

Konstrukci Dispenseru tvoří z velké části kompozitní sendvičové panely a jejich sestava reprezentuje tuhost celé struktury. Protože tuhost sendvičového panelu lze regulovat několika způsoby, existuje i víc možností jak optimalizaci provést. V kapitole věnující se samotné optimalizaci jsou tyto možnosti jedna po druhé zhodnoceny a nakonec vybrána jedna varianta optimalizace, která je později uskutečněna. I přesto, že v začátku nebylo příliš jasné, jak se konstrukce z hlediska tuhosti chová a jak jednotlivé konstrukční celky k celkové tuhosti přispívají, nakonec optimalizace vedla k poměrně jednoduchému řešení.

Ukazuje se, že mnohdy tuhost nejde ruku v ruce s celkovou pevností konstrukce. I přesto, že optimalizovaná varianta Dispenseru již splňuje požadavky na vlastní frekvence, je třeba celou konstrukci přepočítat také z hlediska pevnosti, čemuž je věnována poslední část práce. V této kapitole je proveden základní pevnostní výpočet pro kvazi-statické zatěžovací stavy plynoucí z podmínek startu a letu rakety Vega-C.

DECLARATION

I declare that I have written the Master's Thesis titled "Small satellite dispenser structural optimization" independently, under the guidance of the advisor and using exclusively the technical references and other sources of information cited in the thesis and listed in the comprehensive bibliography at the end of the thesis.

As the author I furthermore declare that, with respect to the creation of this Master's Thesis, I have not infringed any copyright or violated anyone's personal and/or ownership rights. In this context, I am fully aware of the consequences of breaking Regulation § 11 of the Copyright Act No. 121/2000 Coll. of the Czech Republic, as amended, and of any breach of rights related to intellectual property or introduced within amendments to relevant Acts such as the Intellectual Property Act or the Criminal Code, Act No. 40/2009 Coll., Section 2, Head VI, Part 4.

Brno

.....

author's signature

ACKNOWLEDGEMENT

I am grateful to Ing. Robert Popela, Ph.D. for being my university advisor through my work on this thesis. I want to thank all of my family, especially my mother and sister, and friends for support and love. I would also like to thank everyone from S.A.B. Aerospace s.r.o. for support, especially to Tomáš Ridoško for being my technical consultant and to Petr Kapoun for making it possible to write the thesis in the company and for allowing me to be the company's intern for almost two years.

Brno

.....

author's signature

This thesis was written in cooperation with S.A.B. Aerospace s.r.o.



Contents

Introduction	14
1 European space activities	15
1.1 European Space Agency	15
1.1.1 ESA's purpose	15
1.1.2 Member States and funding	16
1.1.3 ESA activities	18
1.1.4 European launchers	20
1.2 Vega-C launcher	23
1.2.1 Launch vehicle history	23
1.2.2 General data and mission profile	23
1.2.3 Launch configurations	25
1.3 SSMS programme	27
1.3.1 SSMS system description	27
1.3.2 Vega PoC flight	28
1.3.3 The future of SSMS	29
1.4 Mechanical environment during launch	29
1.4.1 Quasi-static loads	30
1.4.2 Dynamic loads	30
1.4.3 Stiffness limits	33
2 Finite element model development	34
2.1 General information	34
2.2 FE model overview	34
2.2.1 Assembly hierarchy	35
2.2.2 Units	37
2.2.3 Coordinate systems	37
2.2.4 Constraints	38
2.3 Used materials	38
2.3.1 Metallic components	39
2.3.2 CFRP composite components	40
2.3.3 Sandwich panels core honeycombs	40
2.4 Used elements and properties	42
2.4.1 1D elements	42
2.4.2 2D elements	42
2.4.3 3D elements	44
2.4.4 Spring elements	44

2.4.5	Mass elements	45
2.4.6	Rigid elements	45
2.5	Model validity checks	46
2.5.1	Pre-processor check	46
2.5.2	Unit gravity loading check	46
2.5.3	Free-free strain energy check	48
2.6	Modal analysis of the default model	48
3	Optimization	50
3.1	Optimization approach	50
3.1.1	Panel overall thickness variation	51
3.1.2	Panel skin thickness variation	51
3.1.3	Panel skin layup or/and fibre properties optimization	52
3.1.4	Core modification	52
3.2	Proposed solution	52
3.2.1	Procedure description	53
3.2.2	Optimization results	56
4	Strength verification	59
4.1	Design loads	59
4.2	Stress evaluation and margin philosophy	60
4.3	Strength verification results	61
4.3.1	Metallic components	61
4.3.2	Composite components	62
4.4	Conclusion and manufacturability analysis	62
	Conclusion	64
	Bibliography	65
	List of abbreviations and symbols	69
	List of appendices	72
	A Optimization results	73
	B Load cases	76

List of Figures

1.1	ESA current logo	15
1.2	Map of ESA Member and Cooperating States [5]	16
1.3	ESA 2020 budget by funding source [7]	17
1.4	ESA 2020 budget by domain [7]	18
1.5	Copernicus logo [9]	19
1.6	Sentinel-2 multi-spectrum observation [9]	19
1.7	ESA launchers. From left: Vega, Soyuz, Ariane 5 ECA [13] (modified)	20
1.8	Vega liftoff from Kourou, French Guiana [14] (modified)	21
1.9	Vega-C stages [19]	23
1.10	Vega-C payload fairing during acoustic tests [21]	24
1.11	Single launch configuration [19]	25
1.12	Dual launch configuration - short and long version of the Vespa-C [19]	26
1.13	Multiple launch configuration - Vampire (far left) and SSMS [19] . . .	26
1.14	SSMS Dispenser configurations overview. From left to right, top to bottom: HEX-1, HEX-2, PLAT-1, PLAT-2, PLAT-3, FLEXI-3, FLEXI-4 [23]	27
1.15	SSMS Dispenser PoC during test campaign in Toulouse, France [24] .	28
1.16	Lower Part of the SSMS Dispenser PoC with auxiliary payloads in SAB premises, Brno, Czech Republic	29
1.17	Sine environment definition plot [26]	31
1.18	Shock environment definition plot [26]	32
2.1	FLEXI-3 for Vega-C	34
2.2	FLEXI-3 FE model with P/L	35
2.3	Hexagonal Module with P/L	35
2.4	Main Deck with P/L	36
2.5	External Rods	36
2.6	Tower Module with P/L	36
2.7	Shear Web Module with P/L	36
2.8	FE model CS	37
2.9	Model constraints	38
2.10	Hexagonal honeycomb core [28]	41
2.11	FE model coloured by element topology: 1D and rigids in green, 2D in blue and 3D in red	42
2.12	2D elements used	43
2.13	3D elements used	44
2.14	Separation device [30]	44
2.15	Typical CONM2 and RBE2 usage	45

2.16	Unit gravity loading - displacement plot	47
2.17	Modal analysis of the default model - displacement plot	49
3.1	Stiffness sensitivity to thickness variation	57
3.2	Mass sensitivity to thickness variation	58
4.1	Maximum von Mises stress for metallic components	61
4.2	Maximum failure index (Tsai-Hill) for composite components	62

List of Tables

1.1	European launchers technical overview (Source: www.arianespace.com)	22
1.2	Vega-C typical mission profile [19] (simplified)	25
1.3	L-QSL values for different flight phases [26] (modified)	30
1.4	Sine environment definition [26]	31
1.5	Shock environment definition [26]	32
2.1	Units	37
2.2	EN AW-6082 and Ti-6Al-4V material properties	39
2.3	M55J-RS36 Pre-preg material properties	40
2.4	3/16-5056-0.001p and 1/8-5056-0.001p material properties	42
2.5	PBUSH property stiffness input	45
2.6	Unit gravity loading check results	47
2.7	Free-free strain energy check results	49
3.1	Sandwich panels relative bending stiffness and weight [37] (modified)	50
3.2	List of configurations	54
3.3	Modelling techniques for composite components	55
3.4	Optimization results	56
4.1	DLL values for dimensioning of the FLEXI-3	59

Introduction

We live in modern times where satellite technologies are part of our everyday life. As technology in general evolves and we are more and more aiming to miniaturize the things around us, it is nowadays possible to build a satellite almost as small as a Rubik's cube, while it is still capable of fulfilling missions of great importance such as Earth observation or conducting in-orbit experiments. With platforms so small, even institutions like universities can afford to build their own satellite.

However, putting a satellite of whatever size into an orbit requires extreme amount of technological effort and thus it is extremely costly in general. Up to date, launchers have been designed to place very small number (mostly one or two) of payloads into an orbit, making the launch cost per satellite unaffordable for smaller customers, meaning even if an institution could build a satellite, they surely would not be able to pay for its launch. Unless it would be a shared launch of multiple satellites.

In recent years there has been a competition among industrial companies across the Europe to participate in European launchers programmes and to develop a system capable of carrying multiple payloads into an orbit in a single launch and deployment sequence. This way the launch is shared among the customers and the launch cost per satellite decreases. But the most innovative solutions often bring challenges to overcome. The design of a satellite carrying structure faces many challenges, some of them being stiffness and strength, as the structure is exposed to extreme mechanical loads during launch of the rocket and its journey to Space.

This thesis is dedicated to the stiffness optimization of such structure. It was written under supervision of engineers from the SAB Aerospace structural department as a solution to a real problem that has been encountered during the design phase of the product.

The thesis is divided into four chapters. The first chapter provides an introduction to the field of European space research and brings necessary knowledge regarding satellite launching. The second chapter is an overview of the computational model development of the satellite carrying structure, as the whole optimization is based on finite element method. The third chapter is the optimization itself, where different approaches are discussed and eventually the analyses are performed. The fourth chapter is dedicated to the strength verification of the optimized variant.

1 European space activities

1.1 European Space Agency

European Space Agency (ESA) is an international organisation currently consisting of 22 Member States, most of them being geographically situated in the European continent. Origin of the Agency dates back to the beginning of 1960s when ELDO (the European Launcher Development Organisation) was established in pursuit of developing and building a heavy launcher. Founding ELDO states were Belgium, France, Germany, Italy, the Netherlands and the United Kingdom.

Joined by Denmark, Spain, Sweden and Switzerland later in 1962, they formed ESRO (the European Space Research Organisation) in order to deal with space scientific missions and develop satellites and spacecraft as well. In 1975, a Convention to merge ELDO and ESRO was endorsed at political level, setting up a new agency called ESA and combining the interests of both predecessor organizations. Finally, this Convention entered into force on 30 October 1980. [1][2]



Fig. 1.1: ESA current logo

1.1.1 ESA's purpose

ESA's programmes through its years of existence have always aimed to find out as much knowledge as possible about Earth, our Solar System and also about the Universe in general by developing spacecraft and satellite-based technologies and services. The ultimate goal of ESA is to unite European states in space research and technology and possibly find space applications for technologies that haven't been originally developed for space purposes. By recommending space activities and objectives to its Member States, ESA is responsible for elaborating and implementing a long-term European space policy. In terms of space research, however, ESA is not limited to Europe, since it also closely cooperates with other space organizations outside Europe, such as NASA (the National Aeronautics and Space Administration) and more. [3]

In addition, ESA is increasingly working together with EU (the European Union). Even though the two institutions are different in terms of organisation, competences, rules and procedures, they share a common aim, which is to make European citizens benefit from space programmes. The cooperation between the two institutions officially started in 2004 when a Framework Agreement was established. [4]

1.1.2 Member States and funding

ESA has currently 22 Member States and 9 Cooperating States (June 2020). Unlike Member States, the Cooperating States have slightly modified and limited privileges, but they can still in some ways participate in ESA projects. Complete lists of the states is as follows [5]:

Member States (marked in dark grey in Figure 1.2): Austria, Belgium, Czech Republic, Denmark, Estonia, Finland, France, Germany, Greece, Hungary, Ireland, Italy, Luxembourg, the Netherlands, Norway, Poland, Portugal, Romania, Spain, Sweden, Switzerland and the United Kingdom.

Cooperating States (marked in mid grey in Figure 1.2): Bulgaria, Croatia, Cyprus, Latvia, Lithuania, Malta and Slovakia.



Fig. 1.2: Map of ESA Member and Cooperating States [5]

There are two types of Agency's activities: mandatory and optional. Mandatory activities are funded by contributions from all Member States and the amount is determined by each country's Gross National Product. Studies on future projects, technology research, shared technical investments, information systems and training

programmes belong to the mandatory activities. In addition, the Member States can decide whether they involve in optional activities and how much they want to contribute to these activities. Optional programmes cover the fields of Earth observation, telecommunications, satellite control, space transportation and all the International Space Station activities along with microgravity research. [6][7]

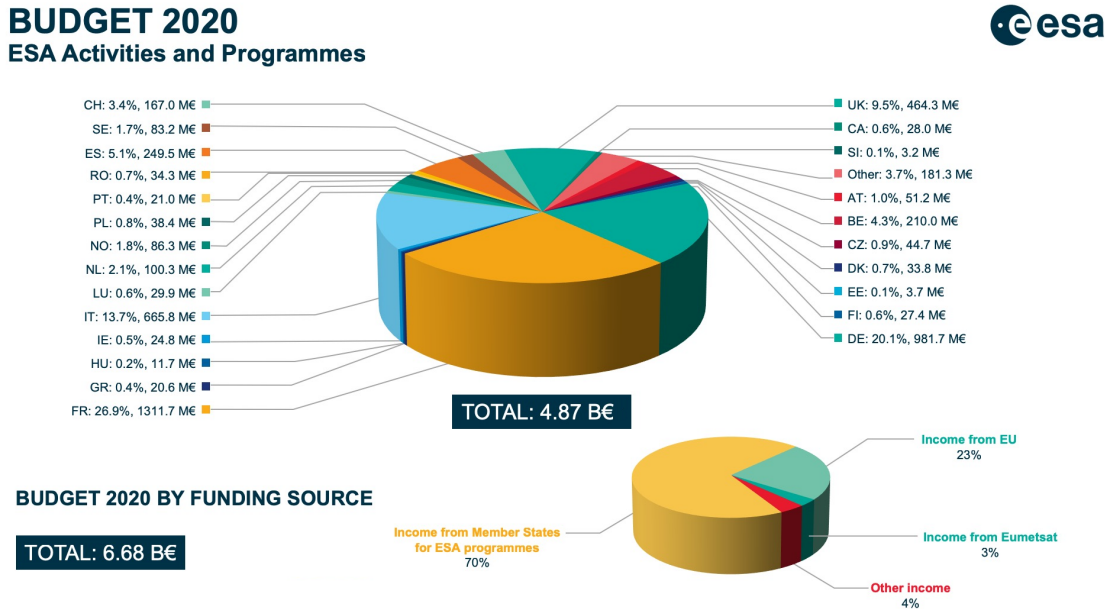


Fig. 1.3: ESA 2020 budget by funding source [7]

As can be seen from Figure 1.3 top pie chart, a total of €4.87 billion comes to ESA in form of Member States contributions. The Czech Republic contribution in 2020 is €44.7 million. It is stated that an average citizen of the Member State pays (in form of taxes) to ESA about the same as the price of a cinema ticket (for comparison this is almost four times lower than in the USA) [6]. With total ESA 2020 budget of €6.88 billion, there are other sources of income. As it is shown in bottom pie chart, 23% comes from EU and 7% from other minor sources.

With its budget ESA works on a principle of geographical return (or often referred to as 'Geo-Return'). Through contracts on space programmes, ESA invests in each Member State an amount equivalent (more or less) to the country contribution. Figure 1.4 shows ESA 2020 budget and its percentage distribution to different programmes in fields of engineering and research. [6]

There are currently around 2200 people working for ESA. These people come from all Member States and work in fields of science, engineering, informational technology or administration. ESA's headquarters are situated in Paris - this is where policies and programmes are decided. Then there is a number of ESA sites in different European countries, one of the most important of them being ESTEC

(the European Space Research and Technology Centre) in Noordwijk, the Netherlands. The others are situated in Spain, Germany, Italy, Belgium and the United Kingdom. [6]

ESA BUDGET BY DOMAIN FOR 2020: 6.68 B€*



*includes activities implemented for other institutional partners

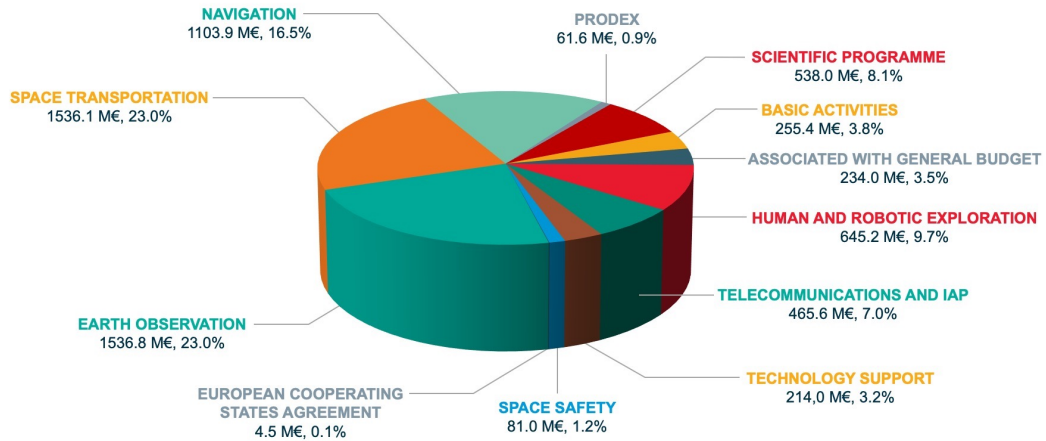


Fig. 1.4: ESA 2020 budget by domain [7]

1.1.3 ESA activities

In order to improve everyday life of the citizens, ESA is putting a lot of effort into providing a reliable base for Earth observation missions, as well as for telecommunication and navigation systems. With scientific missions ESA goes way beyond Earth's orbit, having active and future missions in fields of the Solar system research, as well as the Universe observation.

With all missions being available in detail in source [8], this section brings only a brief overview of two most widely known programmes: *Copernicus* and *Galileo*.

Copernicus

Copernicus is European most ambitious Earth observation programme. It provides accurate and real time data about the Earth's surface, oceans and atmosphere for scientific purposes. [9] However, since the data from Copernicus programme are free-of-charge, everyone can benefit from them. Thanks to this accessibility of

the data and rising interest in space research in general, a large number of individuals or small companies have been setting up their business on evaluating and making interesting use-cases of the satellite data from the Copernicus programme.

ESA is currently in the process of designing and operating a new family of satellites called Sentinels specifically for purposes of Copernicus. Some of them are already in orbit, others are still in the development process. Sentinel-1A and Sentinel-1B (launched in 2014 and 2016 respectively) provide all-weather day and night radar images of the landscape. Direct optical observations are provided by Sentinel-2A and Sentinel-2B (launched in 2015 and 2017 respectively), equipped with visible light, near-infrared and short-wavelength infrared instruments. The two Sentinel-3 (launched in 2016 and 2018 respectively) satellites deliver data for services relevant to the oceans. All Sentinels mentioned above are orbiting the Earth in so called twin-satellite constellation. There is an additional single satellite - Sentinel-5P launched in 2017 - dedicated to atmospheric research. The rest of the Sentinels (4, 5 and 6) are still in development process and will be launched in near future. [9]



Fig. 1.5: Copernicus logo [9]

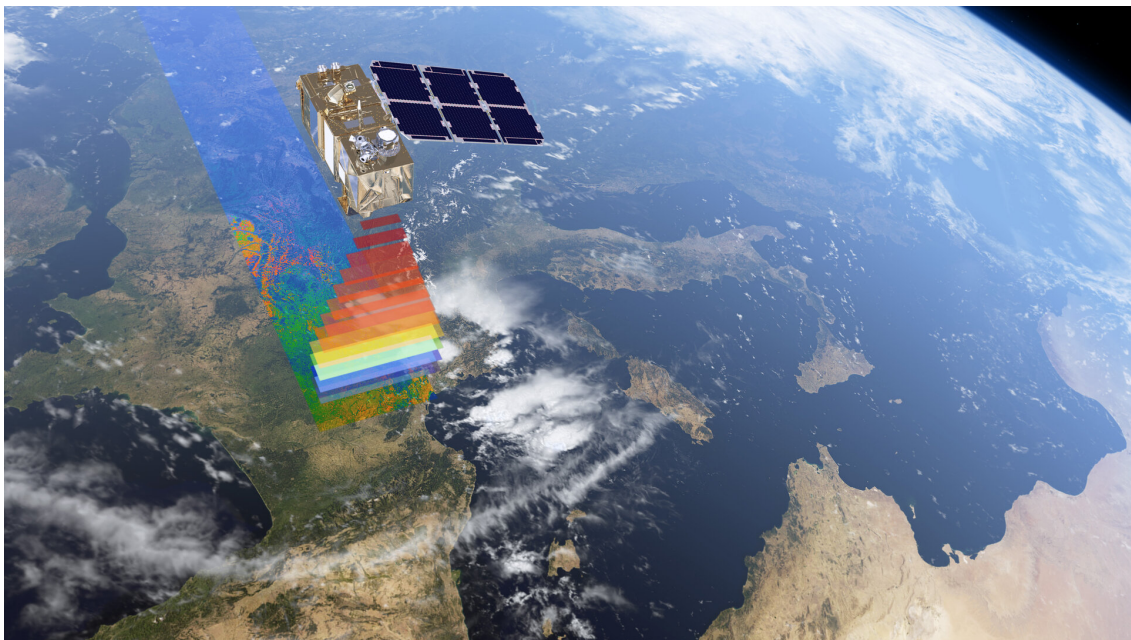


Fig. 1.6: Sentinel-2 multi-spectrum observation [9]

Galileo

Galileo delivers highly accurate positioning service and is a direct alternative to United States GPS and Russian Glonass navigation systems¹. With new technologies and instruments, Galileo can provide real-time positioning accuracy down to the metre range. [10]

After years of testing, the service became available at the end of 2016. The system is currently in operation, but still not fully deployed. When all the satellites are launched, Galileo will consist of 30 satellite constellation from which 24 will be operational and 6 in-orbit spares. The satellites will be positioned in three circular Medium Earth Orbit (MEO) planes. [10]

1.1.4 European launchers

More than 50 years ago by founding ELDO it was initially decided that Europe needed its own family of launchers. The idea was to establish autonomous and reliable access to space in order to start benefiting from it. At present - thanks to this initiative - Europe indeed has its fleet of launchers capable of satisfying institutional and commercial needs. On top of that, Europe's own spaceport has been built in French Guiana, South America. [11]

The responsibility for design, development and manufacture of the European launchers is divided into a number of industrial companies across Europe. For each launcher, one prime contractor is chosen to have supervision over the subcontractors. Arianespace - as the European space transportation company - is linked to ESA by a convention and is in charge of the procurement of the launchers from the prime contractors, marketing and the launch itself. ESA is responsible for the overall management of the launcher programmes. [12]



Fig. 1.7: ESA launchers. From left: Vega, Soyuz, Ariane 5 ECA [13] (modified)

¹Galileo is still interoperable with these systems

Vega

As the smallest launcher from the European fleet, Vega is nominally designed to place 1500 kg payload to 700 km-altitude orbit at 90° inclination. Mass of the payload can vary according to a desired type of orbit or its altitude. Vega is the most suitable launcher for majority of scientific and Earth observation missions. [14]

Vega is a 4-stage rocket with three solid-propellant stages and one liquid propellant stage on top. This upper stage provides attitude and orbit control and secures payload deployment. What makes Vega unique among other small launchers is the fact that it is able to carry multiple payloads. [14]



Fig. 1.8: Vega liftoff from Kourou, French Guiana [14] (modified)

Ariane 5

Ariane 5 is Europe's heavy launcher. Its current version Ariane 5 ECA can carry up to 10 metric tonnes into Geostationary Transfer Orbit or even heavier payloads into Sun Synchronous Orbit (it can handle dual launch configuration). Ariane 5 consists of two stages (central and upper) based on liquid propellant and two side-boosters with solid propellant. [15]

Soyuz

With Vega and Ariane being two opposites as far as payload mass is concerned, usage of medium-class launcher like Soyuz was an opportunity for ESA to complement their family of launchers. This is why it was European interest to start a cooperation on

launchers with Russia. The result of this cooperation was first Soyuz liftoff from European spaceport in French Guiana in 2011. [16]

The Soyuz vehicle used in French Guiana is the version called Soyuz-ST. It has improved performance and benefits from the French Guiana spaceport latitude. Thus it is able to carry more than 3 metric tonnes to Geostationary Transfer Orbit (when launched from Baikonur in Kazakhstan it can carry only 1.7 metric tonnes to the same type of orbit). [16]

Vega-C, Ariane 6

Based on progressively higher demands in space industry it was decided by ESA Member States in 2014 that the Europe needed a more powerful version of the Vega launcher. The main goals are to increase the performance and to reduce the operating costs of the Europe's lightest launcher, as well as to explore the possibilities of carrying more satellites in a single launch. Vega-C is expected to debut in 2020. [17] Since the aim of this thesis is an optimization of a multiple satellite carrying structure for Vega-C, there is a standalone section 1.2 dedicated to description of this launcher.

Not only in case of Vega launcher, but also in case of Ariane the decision was taken in 2014 to start development of a new version - Ariane 6. It is again Europe's response to fast changing commercial launch service market. The rocket will be available in two versions depending on the required mission - Ariane 62 with two side-boosters or Ariane 64 with four. [18]

Table 1.1 shows basic technical data for the whole European fleet.

Tab. 1.1: European launchers technical overview (Source: www.arianespace.com)

Launcher	Height	Fairing \varnothing	Liftoff mass	P/L ¹ to SSO ²	P/L to GTO ³
Vega	29.9 m	2.6 m	137 000 kg	1 500 kg	-
Vega-C⁴	35.0 m	3.3 m	210 000 kg	2 200 kg	-
Soyuz	46.2 m	4.1 m	308 000 kg	4 400 kg	3 250 kg
Ariane 5	50.5 m	5.4 m	780 000 kg	20 000 kg	10 000 kg
Ariane 6⁴	60.0 m	5.4 m	900 000 kg	N/A	11 500 kg

¹ Payload

² Sun Synchronous Orbit

³ Geostationary Transfer Orbit

⁴ These launchers are still in development phase. Technical and performance data are preliminary.

1.2 Vega-C launcher

1.2.1 Launch vehicle history

Vega-C predecessor Vega has its origins in the 1990s, when the Italian Space Agency started investigating the possibility of using Ariane solid booster technology to develop a small launch vehicle. After years of setting up activities and requirements consolidation, the Vega programme was approved by ESA and officially started in 2000. It took more than 10 years of development for Vega to finally launch in 2012 for the first time. Not very long after the inaugural flight of Vega a development of Vega-C has begun as a reaction to an immensely fast-growing market [19].

1.2.2 General data and mission profile

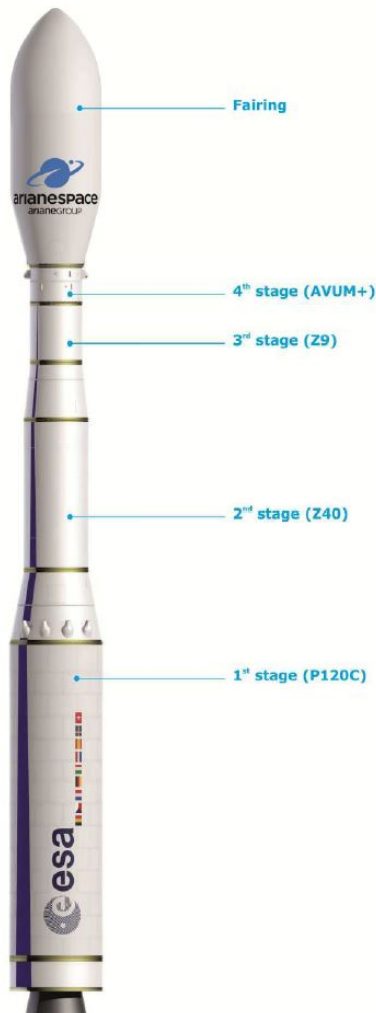


Fig. 1.9: Vega-C stages [19]

Vega-C is a 4-stage launcher (see Figure 1.9) and primarily consists of the following parts [19]:

- Three lower stages based on solid propellant
- Upper stage AVUM+ (Attitude and Vernier Upper Module) based on liquid propellant
- Payload fairing
- Carrying structure for satellites (adapter or dispenser)

The Vega-C **first stage** is powered by a **P120C** solid rocket engine. It contains 141 634 kg of the propellant, delivers maximum vacuum thrust of 4 323 kN and burns for 136 s prior to being separated. [19] [20]

The **second** and **third stage** are **Zefiro Z40** and **Z9** engines. Loaded with 36 239 kg and 10 567 kg of solid propellant they deliver maximum vacuum thrust of 1 304 kN and 317 kN with burn times of 93 s and 120 s. [19] [20]

The **AVUM+** is the **fourth and last stage** and is based on liquid propellant. Its purpose is to provide final orbital maneuvers, ensure the precise pointing of the satellites and eventually perform the orbital injection. It is powered by a reignitable engine which delivers 2.45 kN of thrust with maximum cumulative burn time of 925 s (up to 5 separate burns). In addition, the AVUM+ is equipped

with 6 hydrazine thrusters in order to control its roll and attitude. With flight control, mission management and telemetry systems, this module is also the electrical centre of the rocket. At the end of each mission, the AVUM+ is safely deorbited to limit the amount of space debris. [19] [20]

The payload fairing is made of two separate shells made of sandwich panels. Its purpose is to protect the payload from aerodynamic drag and acoustic pressure (see Figure 1.10) during atmospheric phase of the launch. Once the launcher leaves the most dense layer of atmosphere, both fairing halves are jettisoned by means of pyrotechnical separation devices. [19]



Fig. 1.10: Vega-C payload fairing during acoustic tests [21]

A typical Vega-C mission consists of three phases. **First phase** is an ascent of the rocket to reach the target orbit. It includes ignition, burnout and separation of all stages as they go from bottom to top. **Second phase** is when AVUM+ performs the necessary maneuvers to provide required orbital velocity and trajectory and to properly point the satellite. **Third phase** is the final AVUM+ burn and its deorbitation. [19]

Main events during an ascent profile in terms of time, altitude and relative velocity are given in Table 1.2.

Tab. 1.2: Vega-C typical mission profile [19] (simplified)

Event	Time [s]	Altitude [km]	Velocity [km/s]
First stage ignition	0	0	0
Second stage ignition	142	60	1.90
Third stage ignition	249	123	4.55
Fairing jettisoning	254	126	4.60
AVUM+ first ignition	448	199	7.55
Spacecraft separation	3427	626	7.63

1.2.3 Launch configurations

What makes Vega-C unique is the fact that it is capable of carrying multiple satellites in multiple launch configurations by means of different payload adapters or dispensers. In next paragraphs a brief overview of the launch possibilities is given also with illustrative pictures.

Single launch configuration

Vega-C in this configuration carries only one spacecraft (see Figure 1.11). Using the full Vega-C payload capacity, it is used for costly and the most demanding missions

with the heaviest satellites that are to be placed into Low Earth Orbit. The spacecraft is integrated on Vega via a 'Vampire' adapter which comes in two versions, the 937 and the 1194 (the numbers represent separation interface diameter). [19]



Fig. 1.11: Single launch configuration [19]

Dual launch configuration

This configuration carries two spacecraft (see Figure 1.12). The lower spacecraft is attached to a lower separation device and encapsulated inside the carrying structure

called 'Vespa-C'. The upper spacecraft is then integrated on top of the adapter. In orbit the upper spacecraft (main passenger) is released first and the carrying structure is jettisoned, revealing the secondary spacecraft inside. [19]

Multiple launch configuration

Multiple launch configuration offers a variety of different scenarios (see Figure 1.13). It is expected to be used for launching one medium sized spacecraft and several small auxiliary passengers. However, via modular design of adapters and dispensers it is possible to perform a launch exactly according to customers needs. The expected adapters are as follows [19]:

- Vampire 937 with towers
- SSMS Dispenser in different configurations



Fig. 1.12: Dual launch configuration - short and long version of the Vespa-C [19]

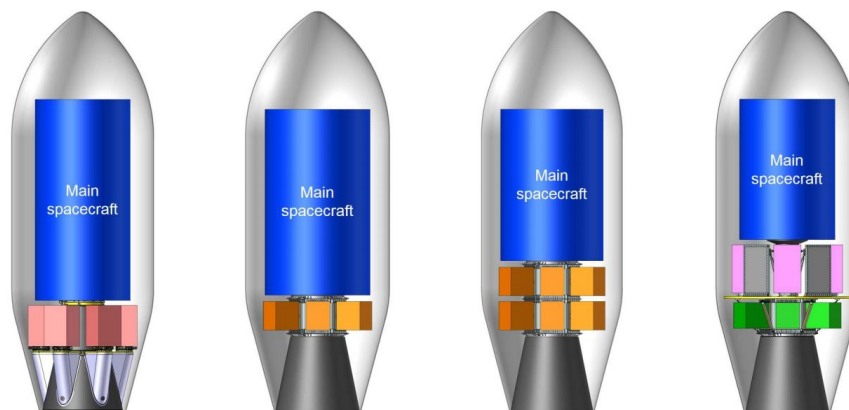


Fig. 1.13: Multiple launch configuration - Vampire (far left) and SSMS [19]

1.3 SSMS programme

Aiming to provide low-cost and regular launch services for small satellites, an initiative called 'Light satellite, Low-cost Launch opportunity (LLL) Initiative' was started in 2016 at ministerial level during ESA Council Meeting. [22] This initiative led to an idea of the Small Spacecraft Mission Service (SSMS) programme. With an ultimate goal of making the access to Space more affordable, a study of technical feasibility was performed and eventually started off the design phase. All the effort was successful and led to manufacturing and testing of the first flight model. [23]

1.3.1 SSMS system description

SSMS Dispenser is a fully modular system which allows accommodation of multiple small satellites and provides their deployment during a shared Vega (or Vega-C in the future) launch. The complete system with dedicated mission preparation processes and procedures is developed by the Vega launcher prime AVIO and under supervision of ESA. The Dispenser structure design authority is SAB Aerospace. [23]

Based on the same structural elements combined in different ways there are several configurations of the Dispenser, as depicted in Figure 1.14.

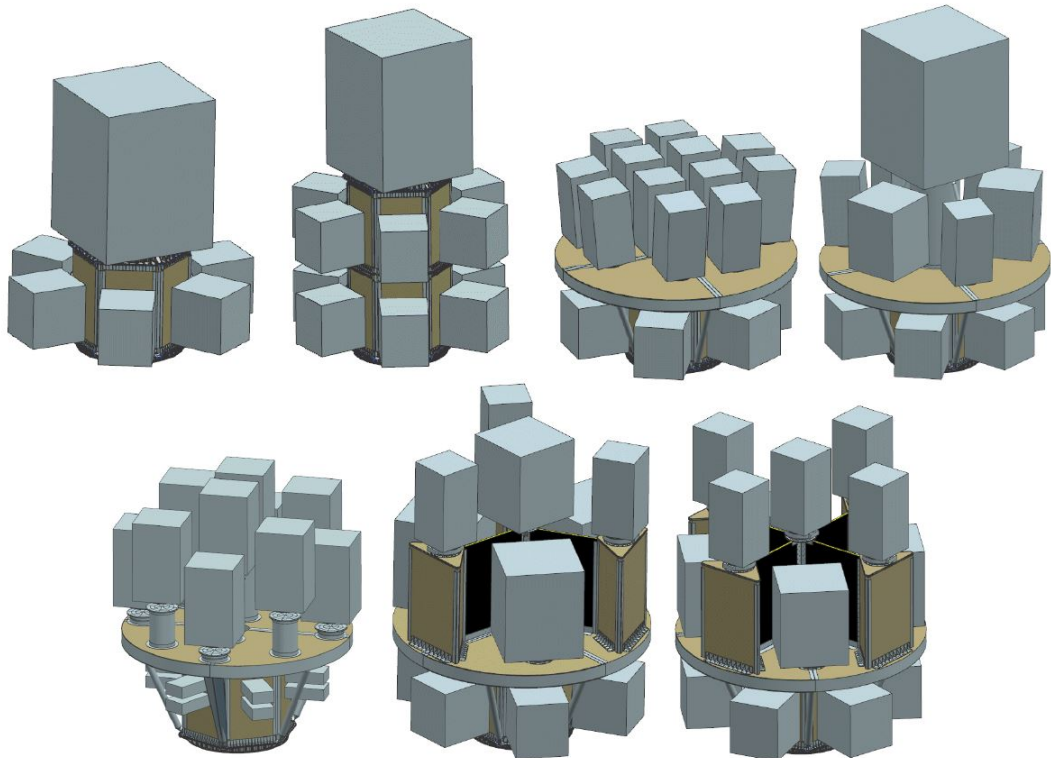


Fig. 1.14: SSMS Dispenser configurations overview. From left to right, top to bottom: HEX-1, HEX-2, PLAT-1, PLAT-2, PLAT-3, FLEXI-3, FLEXI-4 [23]

1.3.2 Vega PoC flight

For the maiden Vega SSMS PoC (Proof of Concept) flight the FLEXI-3 configuration was chosen, based on market survey and small satellite customers demands. Originally scheduled for September 2019 (Vega flight VV16), the flight was postponed due to Vega VV15 failure and rescheduled for March 2020, but was cancelled once again because of the Covid-19 disease pandemic.

During the SSMS PoC development phase the flight model of the FLEXI-3 configuration was designed and analyzed in detail. Prior to design itself a pre-development test campaign was conducted in order to validate critical parts (mostly composite components) manufacturing processes. [23] After successful closure of the design phase, all parts were manufactured and delivered by suppliers from Italy and Czech Republic. The whole structure was integrated in SAB Aerospace facilities in Brno, Czech Republic. After finishing system level test campaign (see Figure 1.15) the Dispenser was officially delivered to AVIO.



Fig. 1.15: SSMS Dispenser PoC during test campaign in Toulouse, France [24]

In cooperation with AVIO and customers, auxiliary payloads (CubeSat deployers) were integrated (see Figure 1.16) on the Dispenser structure for the first time in history on the European continent. Up until now, it has always been done in French Guiana spaceport facilities as a part of pre-flight preparations. PoC integration activities of secondary payloads still remained in South America though.

1.3.3 The future of SSMS

In parallel with Vega-C development, an advanced version of the SSMS Dispenser is in finalisation phase of the design. Vega-C version of the adapter will provide additional payload capacity and will be available in all configurations depicted in 1.3.1. It is expected that the SSMS will be used for launches on a regular basis approx. twice a year.

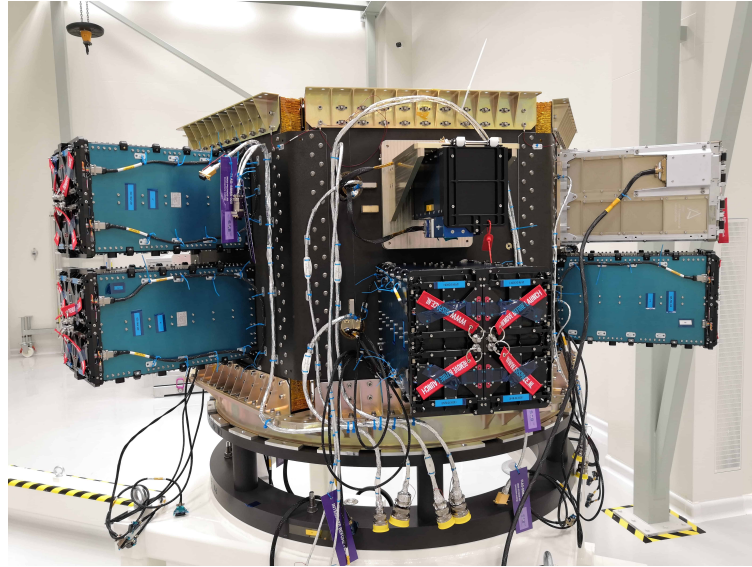


Fig. 1.16: Lower Part of the SSMS Dispenser PoC with auxiliary payloads in SAB premises, Brno, Czech Republic

1.4 Mechanical environment during launch

Launch vehicles in general are tall and slender multi-body or mono-body launchers designed in a way to withstand extreme loads during flight. The primary task of the launcher is to place the payload into an orbit safely and in fully operational state. [25] Thus it is clear that also the payload itself (and its carrying structure, if any) shall not fail structurally or in any other way when subjected to launch, flight or deployment conditions. For engineers it is a challenging task to allocate minimum mass to the structure of the satellite and to comply with stiffness and strength limits at the same time.

Each launcher has usually its user own manual which is publicly available. Among other things it contains information about a variety of mechanical, thermal and also electromagnetic environments to which the spacecraft is exposed during flight (these are the conditions that the payload has to withstand). The environmental conditions in these manuals are, however, applicable only to certain types of

payloads and carrying adapters/structures. When it comes to more complex structures like SSMS, the prime contractor usually defines slightly modified set of requirements to the subcontractor. These requirements are based on the data from user manual but they may be different in some ways. To avoid any misunderstandings it shall be noted that all mechanical environment data (SSMS functional requirements) defined in following sections come from document provided by AVIO [26] and not from Vega-C User’s manual [19].

1.4.1 Quasi-static loads

The dimensioning of the SSMS Dispenser for the Vega-C shall be done using quasi-static loads (QSL). The structure is exposed to steady-state accelerations in longitudinal direction during different phases of the flight and also lateral accelerations caused by blast waves, wind gusts and by controlling the thrust vector. [25]

L-QSL

L-QSL (Launcher QSL) are accelerations transmitted from the vehicle to the structure having their origin in aerodynamics (gusts, transonic buffeting) and propulsion (thrust buildup). They are applied on assembly (the Dispenser with payload attached) CoG (Center of Gravity) and the values are expressed in units of gravitational acceleration (g). [19] The values are defined in Table 1.3.

Tab. 1.3: L-QSL values for different flight phases [26] (modified)

Load event	QSL [g]		
	Longitudinal		Lateral
	Minimum	Maximum	
Lift-off	−4.50	+3.00	±1.35
Max. dynamic pressure	−4.30	+3.00	±0.90
1 st stage flight	−5.00	+1.00	±0.70
2 nd stage flight	−5.00	+3.00	±1.30
3 rd stage flight	−6.70	N/A	±0.20
AVUM+ flight	−1.00	+0.50	±0.70

1.4.2 Dynamic loads

Even though QSL are important for the structure sizing, the launch of a rocket is also very severe environment in terms of dynamic loads. It shall be proven by

analyses and tests (test loads are usually multiplied by an additional test factor) that the structure will survive these loads. [25]

Low frequency environment

Low frequency environment is defined by harmonic excitations at the interface between the launch vehicle and the structure. These vibrations during liftoff and flight are of sinusoidal trend, thus the loads are often called sine environment. The values are usually defined in frequency bands up to 100 Hz. [25] For the Dispenser they are defined in Table 1.4 and Figure 1.17.

Tab. 1.4: Sine environment definition [26]

	Longitudinal		Lateral	
Frequency band [Hz]	5–35	35–110	5–30	30–110
Acceleration amplitude [g]	0.80	1.00	0.80	0.50

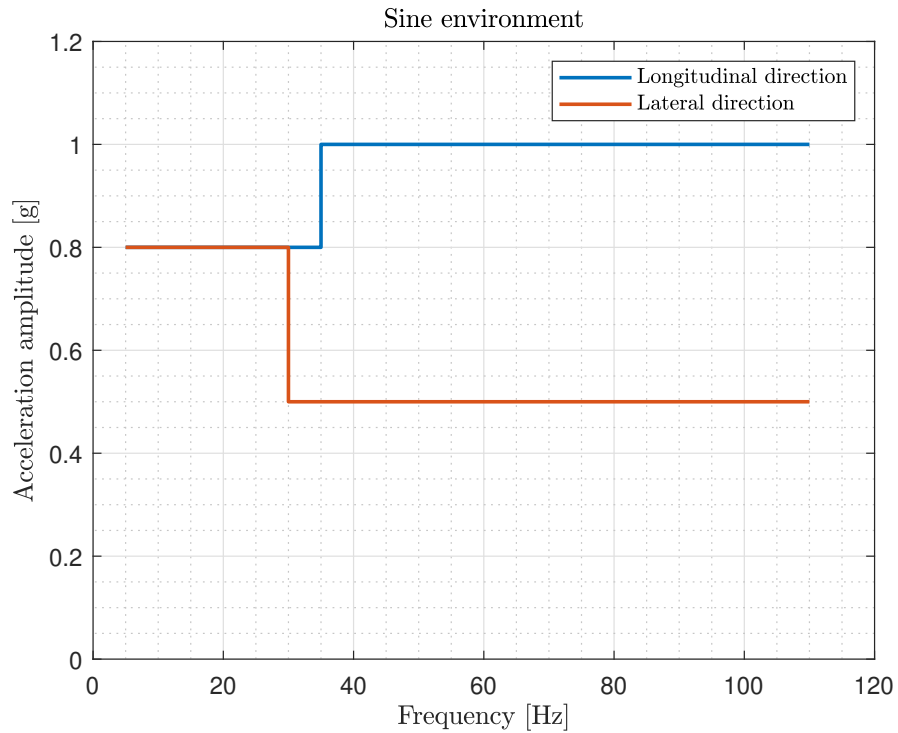


Fig. 1.17: Sine environment definition plot [26]

Shock environment

During flight, stages of the launcher are one by one separated after the fuel burnout in order to make the transportation as efficient as possible. Due to these sudden events - for a fraction of a second - the whole structure is subjected to extreme load peaks called shocks. Shock loads are defined by a SRS (Shock Response Spectrum). These loads may also be induced by fairing jettisoning, engine ignitions and cut-offs and separations of spacecraft by means of pyrotechnical devices.[25] For the Dispenser the shock loads are defined at the interface between the launch vehicle and the Dispenser bottom flange (see Table 1.5 and Figure 1.18).

Tab. 1.5: Shock environment definition [26]

Frequency [Hz]	Shock level [g]	
	Longitudinal	Lateral
100	30	30
1500	1000	1000
10000	1000	1000

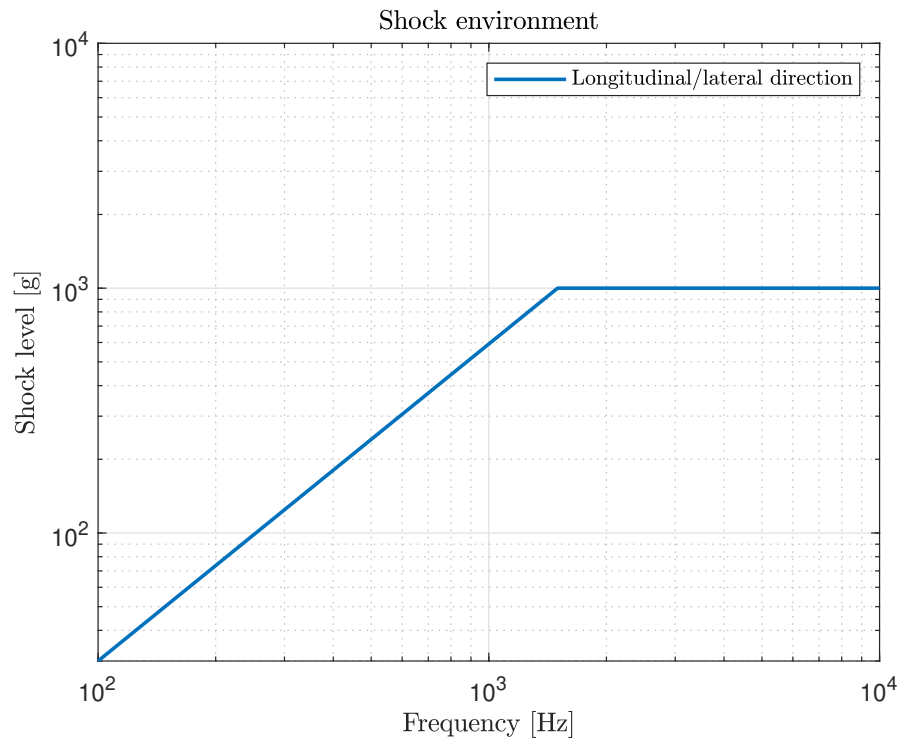


Fig. 1.18: Shock environment definition plot [26]

Acoustic and random environment

During liftoff, rocket engine exhaust noise generates pressure fluctuations under the fairing, exposing the payload to high levels of acoustic loads. Same goes for the transonic flight phase, when these acoustic loads have their origin in aerodynamics phenomena like shock waves or boundary layer turbulence. [19] Acoustic loads can induce mechanical vibrations of random character in the structure.[25].

1.4.3 Stiffness limits

Considering the aim of this thesis, the stiffness requirements for the fully loaded Dispenser are the most important requirements to watch. In most cases, by stiffness it is meant the minimum natural frequencies in lateral and longitudinal directions under specific boundary conditions - fixed at the launch vehicle adapter interface. The minimum natural frequencies are defined to avoid dynamic coupling between the launch vehicle and the payload, which could potentially lead to resonance and structural damage. [25] Based on functional requirements in [26], the Dispenser assembly main natural frequencies (modal effective mass higher than 20%) shall be as follows:

- **lateral frequency:** $f_{lat} \geq 12 \text{ Hz}$
- **longitudinal frequency:** $f_{ax} \geq 51 \text{ Hz}$

The modal effective mass measures the importance of a particular mode shape. The higher the effective mass, the more important the mode shape is in terms of global displacements and reaction forces at the interface where the structure is excited. Low effective masses, on the other hand, imply only local resonances of the structure leading to negligible displacements and low reaction forces. [27]

In frame of the SSMS Dispenser FLEXI-3 configuration (for Vega-C) development phase it was found out during latest design loops that the design of the Dispenser did not comply with stiffness requirements defined above. Therefore, it is necessary to again analyze current design in detail in terms of natural frequencies and to propose design changes, which will lead to meeting the stiffness requirements. The proposed changes shall be minor and they shall cause minimum mass increase.

Next chapter is dedicated to a FE model development and to a modal analysis of the current design.

2 Finite element model development

In this chapter, a detailed overview of the FE model (called *the default model* from now on) creation is given in terms of used elements, materials and properties. The modal analysis of the default model is then presented at the end of the chapter. Used software is herein listed:

- **Pre-processor** (FE mesh preparation): HyperMesh 10.1
- **Solver** (Modal and linear static analyses): MSC Nastran 2017.1
- **Post-processor** (Visualisation): HyperView 10.1

2.1 General information

The Dispenser in FLEXI-3 configuration is, in essence, a payload adapter, thus its task is to be light, provide as much space for the satellite accommodation as possible and be able to withstand all the defined loads. For mass, stiffness and strength driven applications like this, composites are usually preferred as primary materials [25] and the FLEXI-3 is no exception. The structure consists of composite sandwich panels connected together by means of metallic brackets and bolted joints. To get an idea of the overall dimensions, see Figure 2.1

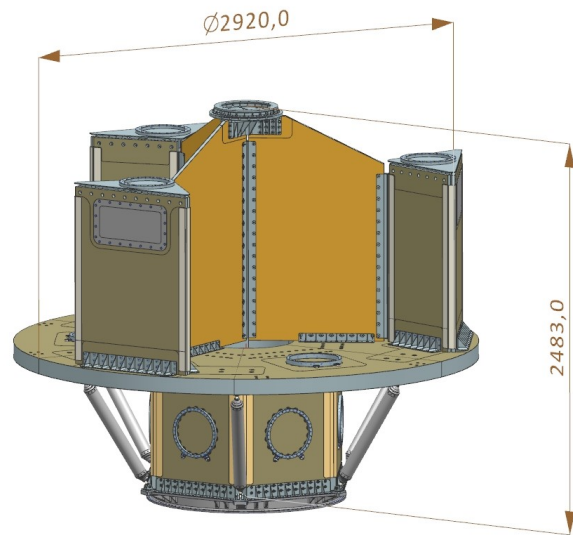


Fig. 2.1: FLEXI-3 for Vega-C

2.2 FE model overview

Finite element model (Figure 2.2) of the FLEXI-3 configuration was created based on current CAD model. Taking advantage of the structure mostly being considered as a thin-walled structure, the vast majority of finite elements are shell elements. In terms of element topology there are some exceptions and they will all be described in detail in relevant sections. The model consists of 351 964 nodes connected to 421 279 elements.

2.2.1 Assembly hierarchy

Different types of composite sandwich panel assemblies divide FLEXI-3 into total of 4 modules:

- **Hexagonal Module (HM)**
- **Main Deck (MD)**
- **Tower Module (TM)**
- **Shear Web Module (SWM)**

HM (Figure 2.3) can be referred to as a base of the structure. On its lower side there is an interface ring which serves for attachment to the Vega-C upper stage. Six side panels accommodate auxiliary payloads.

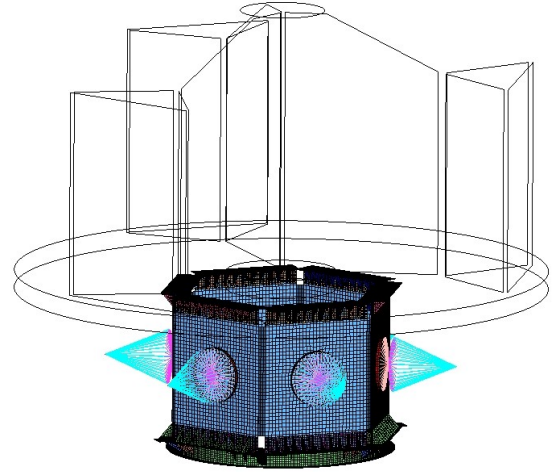
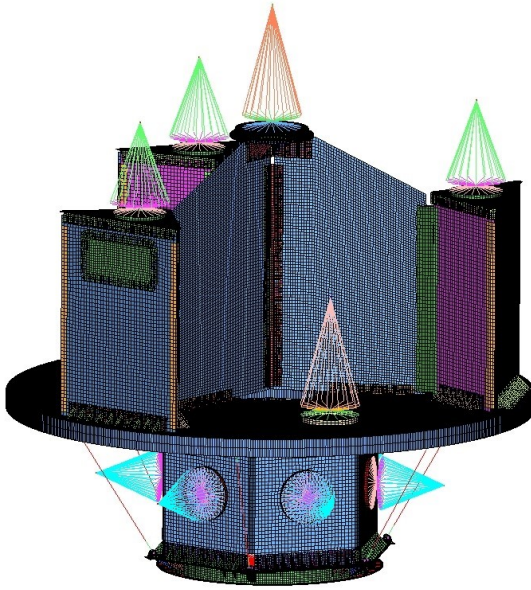


Fig. 2.2: FLEXI-3 FE model with P/L **Fig. 2.3:** Hexagonal Module with P/L

MD (Figure 2.4) is the central platform connecting HM and upper modules. With its 100 mm thickness it is the most robust sandwich panel there is in the whole structure. It provides three positions in 120 degree pattern for accommodation of secondary payloads. Additionally, on its lower face there are six interface points for stiffening struts called **External Rods** (Figure 2.5).

Since FLEXI-3 is a codename for a configuration with three towers, there are three additional positions for secondary payloads on top of the TM (Figure 2.6). SWM (Figure 2.7) panels close the structure, creating a last position for one secondary payload (the heaviest one).

In conclusion, FLEXI-3 can accommodate total of 13 individual payloads. Total mass applied to the FE model according to a CAD mass budget is 2271 kg, where 461.5 kg belong to the structure itself and the rest is allocated to the payloads.

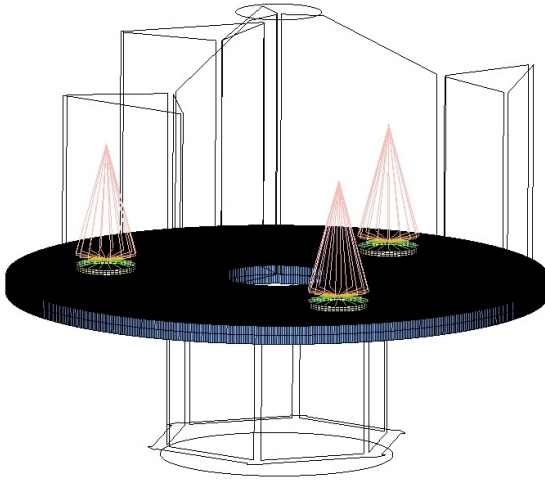


Fig. 2.4: Main Deck with P/L

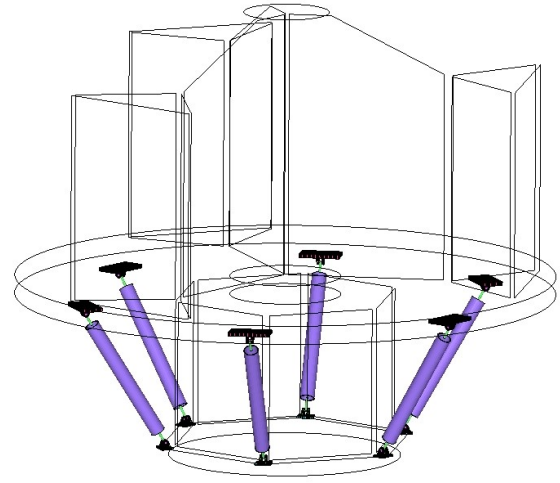


Fig. 2.5: External Rods

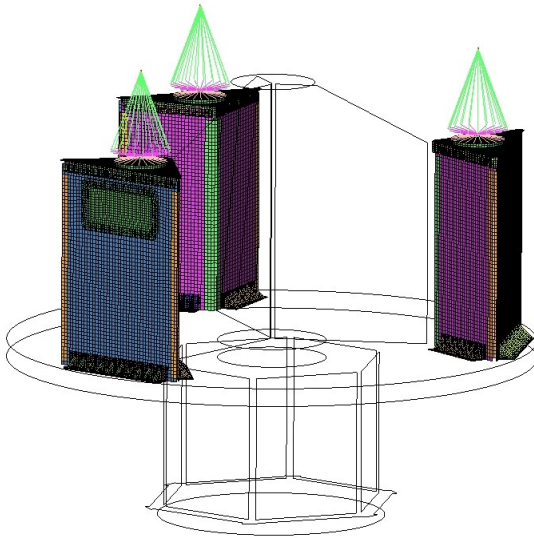


Fig. 2.6: Tower Module with P/L

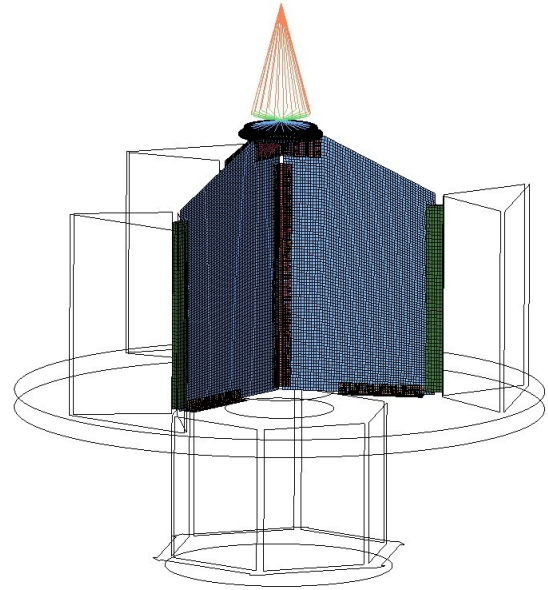


Fig. 2.7: Shear Web Module with P/L

2.2.2 Units

All inputs given to the software shall be based on the SI units (see Table 2.1). [33]

Tab. 2.1: Units

Length/displacement	[m]
Mass	[kg]
Modulus/stress	[Pa]
Density	[kg/m ³]
Axial/shear stiffness	[N/m]
Rotational stiffness	[N·m/rad]

2.2.3 Coordinate systems

In sections 1.4.1 through 1.4.3 it was declared that the loads are applied to the structure in two main directions. Due to this fact it is necessary to first define a global coordinate system (Figure 2.8a) prior to any analyses. The global CS is related to overall displacement assessment, description of the mode shapes resulting from modal analysis and, most importantly, to the load definitions. Besides the global

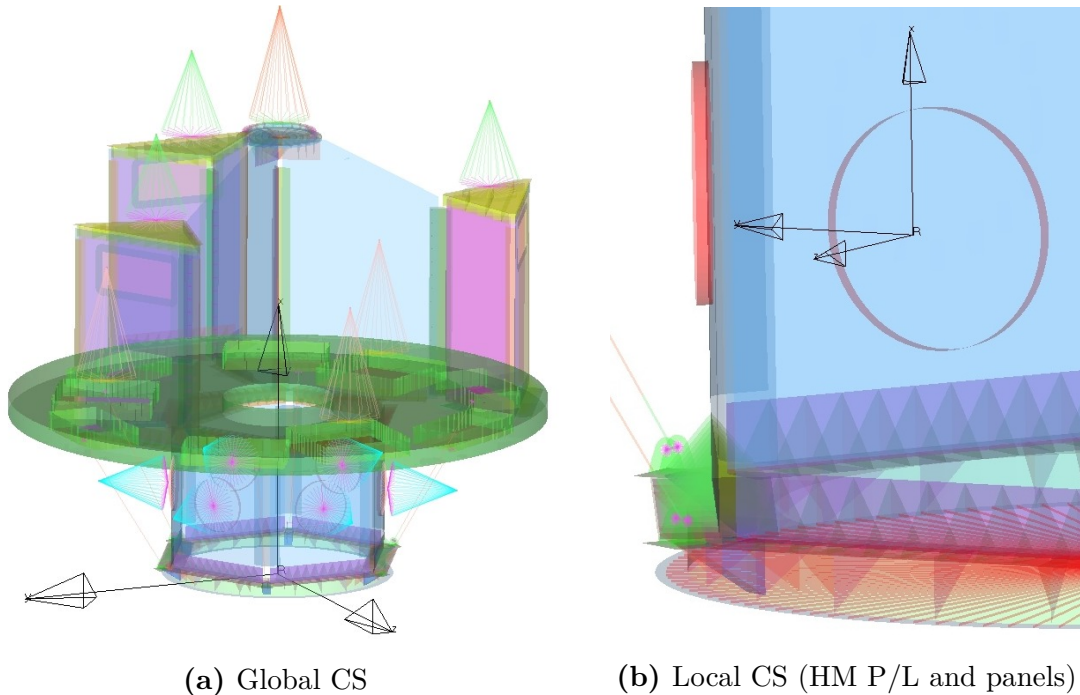


Fig. 2.8: FE model CS

CS, a number of local CS (see an example in Figure 2.8b) were specified primarily to determine material orientations, spring element orientations or P/L positions. Described in detail, the global CS (cartesian) is defined as follows:

- **Origin** of the system is the CoG of the structure projected to the launcher interface plane
- **X-axis** represents the flight direction (vertical axis in Figure 2.8a) and is called the *longitudinal* axis
- **Y-axis** is the first *lateral* axis
- **Z-axis** is the second *lateral* axis and completes the right-handed coordinate system

2.2.4 Constraints

In order to simulate attachment to the launcher as closely as possible, lower interface ring nodes were connected to a central one by means of rigid element (RBE2) spider. A Single Point Constraint (SPC) was then set to this central node, removing all six degrees of freedom (three translations in X, Y and Z direction and three rotations about the global coordinate system axes). This is a typical constraint introduced to FE models used for verification of launch conditions.

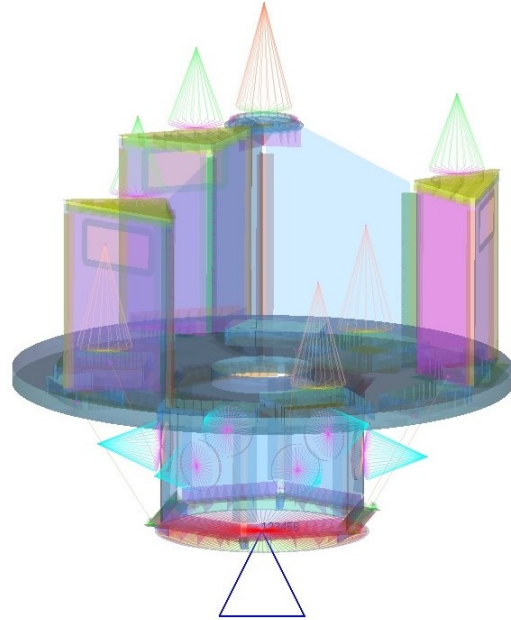


Fig. 2.9: Model constraints

2.3 Used materials

Since the very beginning of space exploration, metallic alloys have been the primary choice as far as materials go. Aluminium alloys have wide range of applications due to their satisfactory strength to mass ratio and excellent machinability. For the most demanding environments from mechanical as well as thermal point of view, titanium alloys are used. [25]

Composite materials play a major role in space industry. In form of CFRP (Carbon Fibre Reinforced Polymer) sandwich panels they are implemented into the systems as load carrying structures, solar panels, antennas and others. The

fiber content and orientation within the composite allow exceptional control of the material properties. [25]

In terms of used material models, the FLEXI-3 is in general composed of the following:

- Metallic components
 - EN AW-6082 (aluminium alloy)
 - Ti-6Al-4V (titanium alloy)
- CFRP composite components
 - M55J-RS36 Pre-preg
- Honeycomb cores
 - 3/16-5056-0.001p (aluminium)
 - 1/8-5056-0.001p (aluminium)

All listed materials and their properties from the Nastran entries point of view are reported in following sections with further explanation, if needed.

2.3.1 Metallic components

Both EN AW-6082 and Ti-6Al-4V are modelled as linear and isotropic materials. For such material model, Nastran MAT1 entry is used. To fully define MAT1, the following shall be input:

- Young's modulus E
- Poisson's ratio μ

Further material properties for 6082 and Ti-6Al-4V, especially design allowables relevant for metallic components stress post-processing and margins of safety calculations, are listed in Table 2.2.

Tab. 2.2: EN AW-6082 and Ti-6Al-4V material properties

	EN AW-6082	Ti-6Al-4V
Young's modulus	70 GPa	100 GPa
Yield strength	255 MPa	880 MPa
Ultimate tensile strength	300 MPa	950 MPa
Poisson's ratio	0.33	0.34
Density	2700 kg/m ³	4430 kg/m ³

2.3.2 CFRP composite components

Uni-directional M55J-RS36 Pre-preg is a typical representative of an orthotropic material, having different mechanical properties in three perpendicular directions. For these purposes, Nastran MAT8 material entry is available. Since it is a material model for 2D shell elements, the third modulus (out-of-plane modulus) is not taken into account. Fully defined MAT8 shall contain the following:

- Tensile modulus ($0^\circ = \text{fiber direction}$) E_1
- Tensile modulus ($90^\circ = \text{matrix direction}$) E_2
- Poisson's ratio μ_{12}
- In-plane shear modulus G_{12}

Summary of all relevant M55J-RS36 properties, either for MAT8 entries or for later post-processing of composite component stresses, is given in Table 2.3.

Tab. 2.3: M55J-RS36 Pre-preg material properties

Tensile modulus 0°	360 GPa
Tensile modulus 90°	7 GPa
Compression modulus 0°	303 GPa
Compression modulus 90°	6 GPa
In-plane shear modulus	5 GPa
In-plane Poisson's ratio	0.3
Tensile strength 0°	1531 MPa
Tensile strength 90°	18 MPa
Compression strength 0°	641 MPa
Compression strength 90°	116 MPa
In-plane shear strength	68 MPa
Density	1650 kg/m ³
Ply thickness	0.125 mm

2.3.3 Sandwich panels core honeycombs

Even though the honeycombs are in fact made of 5056 or similar aluminium alloys, their overall elastic properties significantly differ from isotropic behaviour. The way honeycombs are manufactured ensures different stiffness in three main directions. The spots where individual thin sheets are adhesively bonded are called nodes and the direction along the nodes is called a L-direction. Then there is a W-direction, perpendicular to the previous one. These two make the honeycomb resistant against

shear loads. The last relevant direction is along honeycomb thickness and it makes the honeycomb resist compression. For better understanding all directions are depicted in Figure 2.10.

In general, a stress in a point of an anisotropic material is given by generalised Hooke's law. Unlike its scalar form for linear isotropic material, the generalised form of Hooke's law is a matrix equation. Taking into account all the elastic constants (elastic moduli) and a strain vector, the solution of Equation¹ 2.1 [29] is a vector of all six (normal and shear) stress components. It is worth mentioning that the 6×6 matrix with the elastic constants is a symmetric one, therefore only the diagonal and the upper half is present.

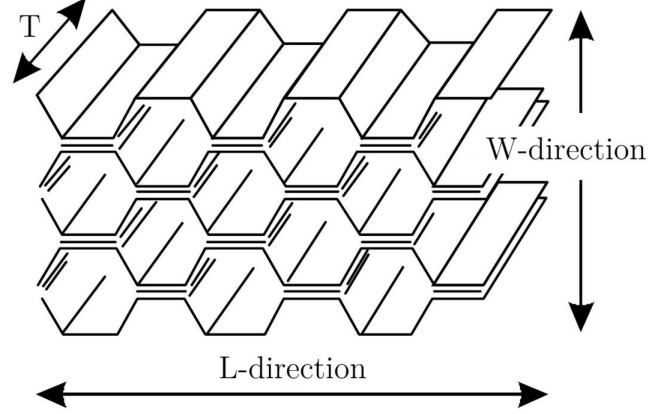


Fig. 2.10: Hexagonal honeycomb core [28]

To match the Equation 2.1, from now on, the L-direction will correspond to x-direction, W-direction to y and thickness to z. As mentioned before, the honeycomb provides stiffness in only three described directions. With all that being said, a term G_{33} represents a compressive modulus of the honeycomb and the G_{55} along with the G_{66} stand for shear moduli in yz and zx directions, respectively.

$$\begin{Bmatrix} \sigma_x \\ \sigma_y \\ \sigma_z \\ \tau_{xy} \\ \tau_{yz} \\ \tau_{zx} \end{Bmatrix} = \begin{pmatrix} G_{11} & G_{12} & G_{13} & G_{14} & G_{15} & G_{16} \\ & G_{22} & G_{23} & G_{24} & G_{25} & G_{26} \\ & & G_{33} & G_{34} & G_{35} & G_{36} \\ & & & G_{44} & G_{45} & G_{46} \\ & & & & G_{55} & G_{56} \\ & & & & & G_{66} \end{pmatrix} \cdot \begin{Bmatrix} \varepsilon_x \\ \varepsilon_y \\ \varepsilon_z \\ \gamma_{xy} \\ \gamma_{yz} \\ \gamma_{zx} \end{Bmatrix} \quad (2.1)$$

From Nastran point of view, the MAT9 entry is applicable to define an anisotropic material. To fully define MAT9 basically means to populate the 6×6 symmetric matrix with elastic constants. G_{33} , G_{55} and G_{66} are known honeycomb properties (see Table 2.4 for actual values) and the rest of the elastic constants are near-zero in values (the honeycomb shows almost no stiffness at all in these directions). However, the zero values cannot be input directly into Nastran, since they cause grid point

¹Thermal loading is not considered in this equation. Otherwise the equation would also contain a thermal expansion coefficient vector and a temperature increment.

singularities. For that reason, small values of 1000 Pa were used to fill in the rest of the matrix to avoid the computational errors.

Tab. 2.4: 3/16-5056-0.001p and 1/8-5056-0.001p material properties

	3/16-5056-0.001p	1/8-5056-0.001p
Compressive modulus	670 MPa	1280 MPa
Shear modulus (L-direction)	310 MPa	480 MPa
Shear modulus (W-direction)	140 MPa	140 MPa
Density	49.7 kg/m ³	72.1 kg/m ³

2.4 Used elements and properties

A detailed look into different element types in terms of topology (see Figure 2.11) and their properties used in the model is given in following subsections.

2.4.1 1D elements

It turns out that the only components where using 1D is beneficial in frame of the FLEXI-3 structure are the External Rods. Pin-supported at each of their ends, the rods were modelled as CBAR elements with six degrees of freedom in each node and assigned with PBAR properties (defining the tubular cross-sections). The advantage of using 1D elements here is obvious - even though the tubes are considered as thin-walled and could potentially be meshed with 2D shell elements, a single 1D element along the length of the rod can satisfactorily substitute high number of 2D elements and save computational time.

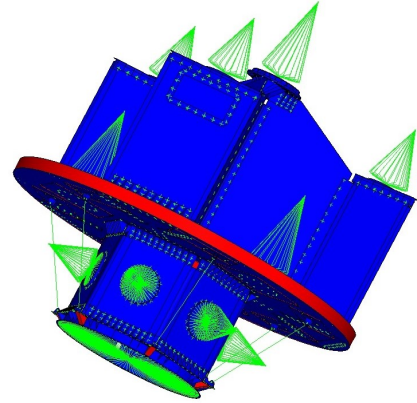


Fig. 2.11: FE model coloured by element topology: 1D and rigids in green, 2D in blue and 3D in red

2.4.2 2D elements

Since the FLEXI-3 mostly consists of structural parts with high surface to thickness ratio, it is advantageous to use 2D elements to mesh the structure. Customer preferred element types are CQUAD4 (Figure 2.12a) quadrilateral isoparametric

elements. Where necessary or unavoidable, CTRIA3 (Figure 2.12b) elements are used. It should be emphasized that CQUAD4 and CTRIA3 have, in default, five degrees of freedom in each node - three translations and two out-of-plane rotations, meaning there is missing stiffness in in-plane direction - often called 'drilling' degree of freedom (depicted in red in Figure 2.12). Since there are countless cases where a component is modelled in such manner that the missing rotational degree of freedom would cause grid point singularities (e.g. T-junctions), it is necessary to artificially introduce this third rotational degree of freedom to the elements. This is done by adding a Nastran parameter `PARAM,K6ROT,100.0` to the solver deck.

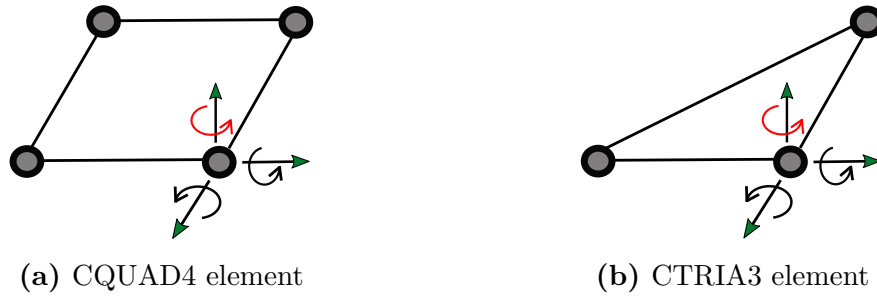


Fig. 2.12: 2D elements used

With the right choice of element property, the 2D modelling technique - compared to usage of 3D elements² - leads to significant computation time reduction while maintaining accuracy. For isotropic components a PSHELL property was chosen, assigning membrane, bending and transverse shear behaviour to the elements. As far as composite components go, a PCOMP property is the most suitable one to define a laminate. The PCOMP gathers information about ply materials, thicknesses and fiber orientations. In principle, it derives equivalent PSHELL entries for composite elements. Pre-preg plies are stacked into laminates and implemented into PCOMP property in following sequence:

- **HM panel skin:** $[0/45/90/-45_2/90/45/0]_S$ - 16 plies with total thickness 2 mm
- **MD panel skin:** $[0/45/90/-45]_S$ - 8 plies with total thickness 1 mm
- **TM panel skin:** $[0/45/90/-45]_S$ - 8 plies with total thickness 1 mm
- **SWM panel skin:** $[0/45/90/-45]_S$ - 8 plies with total thickness 1 mm
- **Monolithic CFRP brackets:** $[0/45/90/-45_2/90/45/0_2/45/90/-45]_S$ - 24 plies with total thickness 3 mm

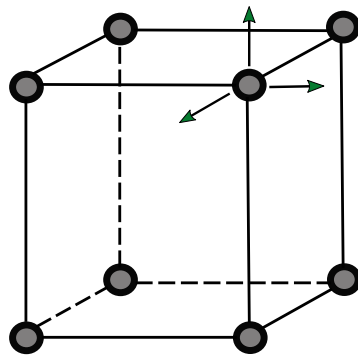
²In many cases, using 3D elements may even cause unsatisfactory results due to having only translational degrees of freedom. In other words, when meshing a thin-walled part with only one layer of 3D elements, the elements are not able to describe bending deformations accurately enough due to missing rotational degrees of freedom. The phenomena can be eliminated by increasing the number of 3D element layers, but at a cost of extreme computational time increase. Consequently, 3D modelling is not very suitable for large models.

2.4.3 3D elements

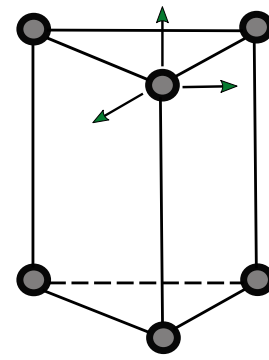
Even though it was possible to model the structure by 2D elements for the most part, there were some areas where usage of 3D elements could not be avoided, such as thick metallic ribs or MD panel core.

Used type of element is the CHEXA (Figure 2.13a), a six-sided isoparametric solid element with 8 nodes. Where necessary, CHEXA elements are complemented with a five-sided version CPENTA (Figure 2.13b). For each of their nodes, both elements provide stiffness in three translational degrees of freedom.

PSOLID properties and material orientation (in case of anisotropic behaviour) were assigned to all solid type element groups.



(a) CHEXA element



(b) CPENTA element

Fig. 2.13: 3D elements used

2.4.4 Spring elements

Use of spring elements is essential when it comes to modelling joints. Majority of spring elements in the FLEXI-3 model are used for bolted joints, only few exceptions are utilised for other purposes, namely for modelling a stiffness of spacecraft separation devices called lightbands (see Figure 2.14).

Used element type is called CBUSH, which is a Nastran spring element providing stiffness in six directions. In all cases it is modelled as a zero-length spring connecting two coincident nodes shared by two different 2D elements.

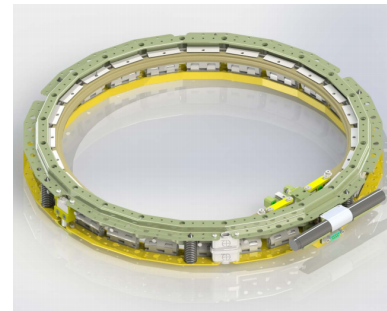


Fig. 2.14: Separation device [30]

Corresponding property for the CBUSH element is a PBUSH, which represents generalized spring and damper. Spring behaviour is enforced via stiffness values input in six directions (three translational and three rotational).

The stiffness values considered for all groups of CBUSH elements are listed in Table 2.5. Data for lightbands (LB) were taken from source [30] (obtained by tests).

Tab. 2.5: PBUSH property stiffness input

CBUSH	Translational stiffness [N/m]			Rotational stiffness [N·m/rad]		
	K1	K2	K3	K4	K5	K6
Joints	1×10^9	1×10^9	1×10^9	1×10^6	1×10^6	1×10^6
11" LB	4.6×10^8	1×10^9	1×10^9	1×10^6	5.0×10^6	5.0×10^6
13" LB	5.1×10^8	1×10^9	1×10^9	1×10^6	6.8×10^6	6.8×10^6

2.4.5 Mass elements

Concentrated mass elements play a major role when loading the FLEXI-3 structure with a weight of satellites. Instead of detailed model, a satellite is replaced by a single CONM2 element situated in the satellite CoG and representing its mass and inertia properties (see Figure 2.15 on top). The element is then attached to the structure by means of rigid elements described in subsection below.

2.4.6 Rigid elements

Unlike all the other element types discussed above, rigid elements are not 'elements' in the true sense. They can be thought of as mathematical formulations defining displacements of multiple nodes - often referred to as MPC (Multi-Point Constraints). For RBE2 element (MPC) type, displacements of multiple nodes (called dependent nodes) are controlled by

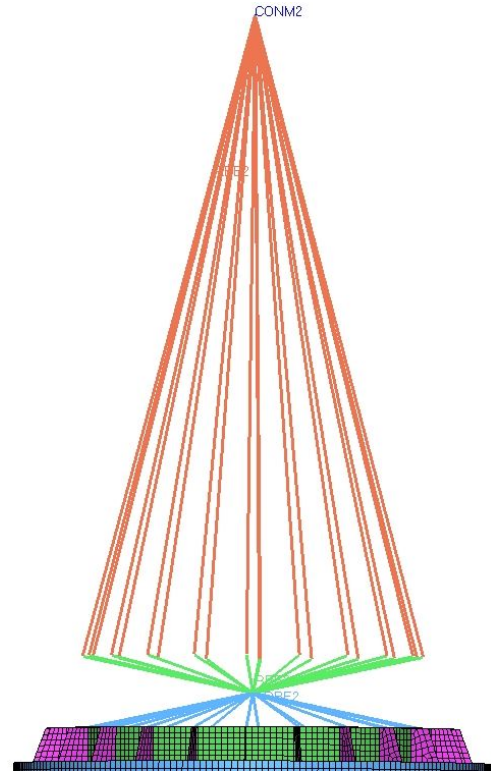


Fig. 2.15: Typical CONM2 and RBE2 usage

displacements of a single one (called an independent node). Consequently, this formulation makes completely rigid connection among the nodes, making the MPC suitable for attaching payloads to the structure (see the rigid spider in Figure 2.15).

Another application of RBE2 is constraining the base of the structure to simulate attachment to the launcher, as described in 2.2.4.

2.5 Model validity checks

In the course of the FE model creation process and imminently after its finalization, before proceeding to structural verification and declaring correspondent results as valid, it is necessary to prove by common-sense checks and mathematical checks that the FE model is accurate and applicable for the analyses.

2.5.1 Pre-processor check

Prior to processing a solver deck for Nastran, the FE model shall be first inspected directly in pre-processing software for potential errors. Elements shall be checked for geometrical distortions (aspect ratio, angles, warping, etc.), connectivity and duplicates. Consistent usage of units and assignment of correct properties, element orientations and coordinate systems are part of the check as well. [31]

The model successfully passed the check, showing no erroneous behaviour and having sufficient mesh quality to proceed to following mathematical checks.

2.5.2 Unit gravity loading check

The purpose of this check is to verify that the constrained FE model provides reasonable displacements and accurate reaction forces when subjected to gravity loading in all three main directions. [32]

Results of this validity check, which is run by a standard Nastran executive deck 'SOL 101' for linear static³ analyses, shall show no large displacements. Also, reaction forces at grounding location extracted by 'SPCFORCES' case control card shall be in line with values obtained by a simple *mass* \times *acceleration* calculation. [32]

³The FE formulation for linear static problems is in form of

$$\mathbf{K}\mathbf{u} = \mathbf{F}, \quad (2.2)$$

which represents a system of linear equations, where \mathbf{K} is a global stiffness matrix composed of sub-matrices corresponding to applied element types, \mathbf{u} is a vector of nodal displacements and \mathbf{F} is a vector of external nodal loads. To put it simply, solving this system of equations for \mathbf{u} provides unknown displacements, eventually leading to structural stress computation.

As a part of this check, a ratio ε for residual work is also computed⁴ and shall not exceed a value of 1×10^{-8} defined by ECSS. [33]

The results are summarized in Table 2.6 with respect to all requirements defined above. Displacements in all three loading directions are also plotted in Figure 2.16, showing no excessive values and making the overall deformed shape look logical and convincing.

Tab. 2.6: Unit gravity loading check results

Reaction forces ¹		Residual work	
Direction	Force [N]	Direction	Epsilon [-]
X	22339	X	2.74×10^{-12}
Y	22339	Y	4.90×10^{-12}
Z	22339	Z	5.04×10^{-12}
Applied ²	22337	Threshold	1.00×10^{-8}
Status	PASS	Status	PASS

¹ Absolute values were taken.

² $F = m \cdot g$

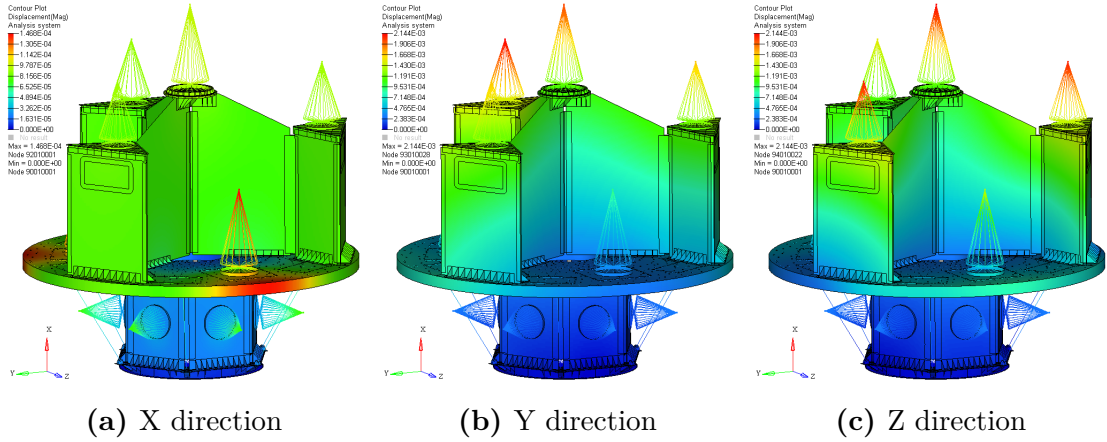


Fig. 2.16: Unit gravity loading - displacement plot

⁴In theory, internal and external nodal forces shall be in equilibrium. FE models often show small deviations, causing residual forces δF to appear. Residual work δW produced by these forces is then compared to the total applied load work W via equation $\varepsilon = \frac{\delta W}{W}$ [33]

2.5.3 Free-free strain energy check

While the previous check was aiming to investigate a static behaviour of the structure, this one deals with a dynamic performance. When unconstrained, the FE model shall act as a rigid body. Running a modal analysis⁵ (Nastran executive deck 'SOL 103') of such free model should reveal six rigid body modes with natural frequencies equal to zero (in theory). [34] According to [33], actual values shall be equal or less than 0.005 Hz.

This check also verifies the model stiffness matrix in relation to any unintentional groundings (incorrectly specified constraints or rigid elements). [34] The verification is done by strain energy⁶ computation (Nastran case control card 'GROUND-CHECK') for the rigid body, which should be again theoretically equal to zero. Based on [33], typical acceptable values of strain energy output from grounding check are, for all translations and rotations, below 0.001 J.

The results are again summarized in Table 2.7.

2.6 Modal analysis of the default model

After successfully passing the checks, the model could undergo a proper modal analysis. For the constrained conditions, all natural frequencies up to 100 Hz were extracted by SOL 103. Particular attention was given to modes with modal effective masses higher than 20% (as mentioned in 1.4.3) in different directions within global CS. First mode to be found exceeding the value was declared to be the first natural mode.

⁵The FE formulation is based on an equation of free undamped vibration

$$\mathbf{M} \frac{d^2 \mathbf{u}}{dt^2} + \mathbf{K} \mathbf{u} = 0, \quad (2.3)$$

where \mathbf{M} is a global mass matrix representing inertia properties of the system, \mathbf{K} is again a global stiffness matrix, \mathbf{u} represents nodal displacement vector and $\frac{d^2 \mathbf{u}}{dt^2}$ is a vector of nodal accelerations.

Assuming a harmonic motion in form of

$$\mathbf{u} = \mathbf{A} \sin(\omega t), \quad (2.4)$$

the Equation 2.3 leads (after differentiation and simplification) to

$$(\mathbf{K} - \omega^2 \mathbf{M}) \mathbf{A} = 0, \quad (2.5)$$

where ω^2 is an eigenvalue and \mathbf{A} is an eigenvector. The Equation 2.5 is called an eigenproblem. Physical representation of eigenproblem solution (finding ω^2 and \mathbf{A}) are the natural frequencies and mode shapes. There are several advanced numerical eigenvalue extraction methods available. In this case the Lanczos method is used. [35]

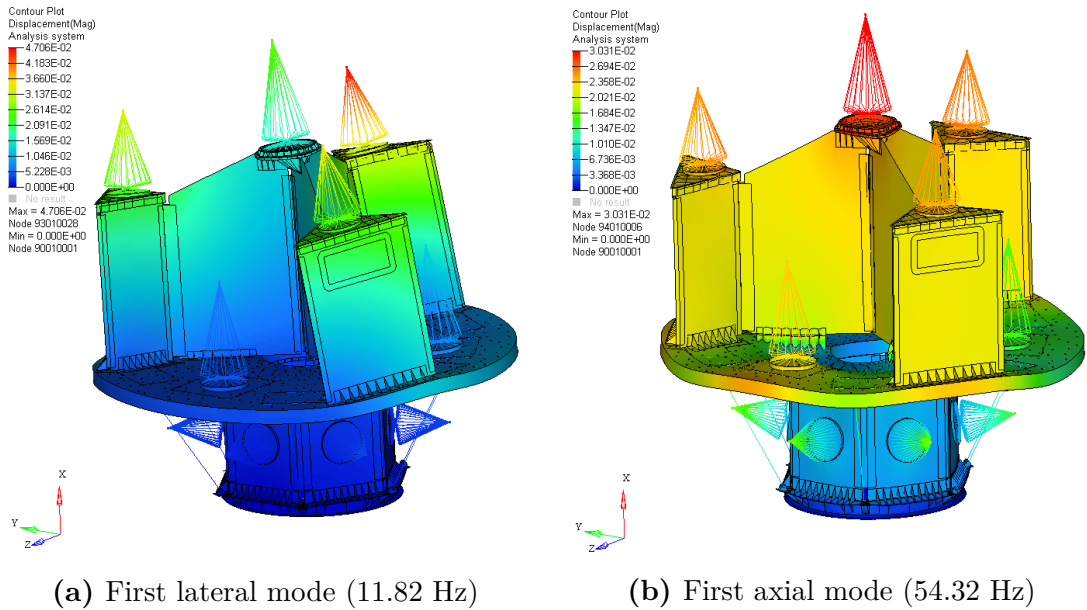
⁶An energy stored in a deformed solid body subjected to external loading. [36]

Tab. 2.7: Free-free strain energy check results

Rigid body motion		Grounding check	
Mode	Frequency [Hz]	Direction	Strain energy [J]
1	4.22×10^{-5}	1	1.45×10^{-4}
2	5.42×10^{-5}	2	6.79×10^{-5}
3	1.12×10^{-4}	3	1.87×10^{-5}
4	1.55×10^{-4}	4	1.17×10^{-4}
5	1.80×10^{-4}	5	1.38×10^{-4}
6	1.89×10^{-4}	6	1.37×10^{-4}
Threshold	5.00×10^{-3}	Threshold	1.00×10^{-3}
Status	PASS	Status	PASS

As depicted in Figure 2.17a, a main mode in lateral direction was found at 11.82 Hz with its effective mass being 51.9% of the total structure mass. For axial direction, first relevant mode appeared at 54.32 Hz with 89.4% effective mass. The mode shape is shown in Figure 2.17b.

While the first axial mode shows compliance with stiffness limit of 51 Hz (with satisfactory margin) defined in 1.4.3, the lateral mode is slightly under the 12 Hz limit.

**Fig. 2.17:** Modal analysis of the default model - displacement plot

3 Optimization


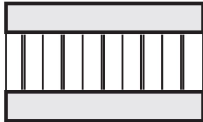
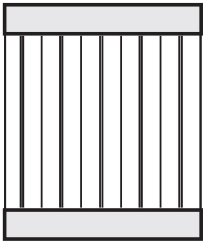
Based on the results regarding natural frequencies from 2.6, this chapter is dedicated to investigation of potential solution to the stiffness problem in lateral direction and the solution itself.

3.1 Optimization approach

As mentioned before, the FLEXI-3 main structural parts are the sandwich panels. Since they are designed to be the crucial components carrying majority of loads and representing the stiffness of the whole structure, an effort will be made in following sections to target and modify their design in such way that the structure's dynamic behaviour will eventually comply with desired first natural frequency threshold in lateral direction.

A sandwich panel can be basically thought of as an I-beam with skins representing flanges of the beam and core representing a web. In general, the skins are present to carry in-plane stresses due to bending and tension. Shear loads are carried by the core. Also, its essential role is to keep a distance between the skins, contributing to the bending stiffness of the panel (see Table 3.1 for properties comparison of panels with different thickness). [38]

Tab. 3.1: Sandwich panels relative bending stiffness and weight [37] (modified)

			
Relative thickness	1	2	4
Relative bending stiffness	1	7	37
Relative weight	1.00	1.03	1.06

However, what makes a sandwich panel slightly different from an I-beam is relatively low shear stiffness of the core. When the panel is subjected to a bending moment caused by a force, the shear deformation contributes to the overall deformation. Therefore, the shear stiffness of the core also contributes to the overall stiffness of the panel and shall not be neglected. [38]

To reduce the deflections (thus stiffen the structure and increase its natural frequency) of the FLEXI-3 first lateral mode, foreseen modifications of the sandwich panels are as follows:

- Overall thickness variation
- Skin thickness variation
- Skin modification
- Core modification

3.1.1 Panel overall thickness variation

This method is based on finding an optimal solution in terms of each FLEXI-3 module (HM, MD, TM and SWM) panel overall thickness, while the individual panels composition remains unchanged (i.e. the panel skins keep the nominal thicknesses defined in 2.4.2 and the core keeps the nominal honeycomb type).

Without further explanation, pros and cons considered for this method are herein listed:

Pros:

- The best results in terms of reducing the weight penalty are foreseen for this method.
- Relatively simple optimization setup - a parametric model with only 4 variable overall thicknesses of the panels.

Cons:

- Additional design modifications (mostly concerning interfaces) of the structure needed due to changes of panel thickness dimensions.
- A need to manufacture 4 different non-standard panel thicknesses, possible manufacturing costs increase.

3.1.2 Panel skin thickness variation

In contrast with the method above, this approach keeps the overall panel thickness unchanged and works with reinforcing the skins by increasing their thickness.

Pros:

- Straightforward calculation of specific number of cases leads to simple analyses without iterations.
- No need of further redesign since the nominal panel thicknesses are kept.

Cons:

- A potential to fully minimize the weight penalty might not be used within this method.
- Possible higher manufacturing costs related to pre-preg consumption.

3.1.3 Panel skin layup or/and fibre properties optimization

With wide range of high-modulus carbon fibres being available on the market, one can improve the pre-preg tensile modulus in main direction and consequently the laminate stiffness at the cost of its strength. Also, a new and possibly a more suitable way of laminate stacking can be discovered. However, this one is very demanding method in terms of both time and difficulty. On top of that, with a different laminate stacking sequence and even with a material modification, a need to conduct a new qualification campaign rises, which proves to be expensive.

Pros:

- A potential to come up with the most balanced laminate properties in terms of both stiffness and strength.

Cons:

- Very challenging optimization setup, high number of variables and high amount of setup and computation time.
- Additional costs related to qualification campaign of new laminate samples.

3.1.4 Core modification

This simple method deals with modification of the honeycomb type for each panel. The honeycombs are available in different cell sizes and sheet thicknesses, where obviously denser honeycomb means higher shear stiffness, thus higher contribution to the overall panel stiffness.

Pros:

- Highly time-saving and simple solution.
- Near-zero additional manufacturing costs.

Cons:

- Higher weight penalty foreseen due to lower influence on the stiffness parameters than in case of the skins and the overall thickness.

3.2 Proposed solution

After considering all the pros and cons of the methods introduced above, a decision to use the **skin thickness variation** method from 3.1.2 was taken. The driving force for this decision was mainly the fact that the structure would not need any redesign after the optimization, since it is related only to the skin modification while preserving total panel thickness, thus not interfering with any existing interfaces or other structural parts. In addition, due to fairly simple and not very time consuming

analyses, the project work and further structural verification can proceed, without the optimization causing a significant delay.

It is also necessary to state that this decision was made in accordance with SAB Aerospace structural department's vision of the overall optimization approach of the FLEXI-3.

3.2.1 Procedure description

A summary of the optimization steps is given in standalone subsections below.

Defining design space

First and the most important step is to define the minimum and the maximum thickness of the skins to work with, as well as the thickness increments between the limits. This is based on several conditions:

- The skin shall be a laminate that has been used previously, either directly in the FLEXI-3 structure or in frame of the whole SSMS project.
- The skin shall be a laminate that shows quasi-isotropic¹ behaviour.
- The first lateral frequency (11.82 Hz) of the default model is quite close to the desired limit of 12 Hz, hence there is no need to go beyond moderate reinforcements of the skins.

Taking into account the conditions above, the thickness values were chosen as follows:

- **1 mm skin** with stacking sequence $[0/45/90/-45]_S$
- **1.5 mm skin** with stacking sequence $[0/45/90/-45_2/90/45/0_2/45/90/-45]$
- **2 mm skin** with stacking sequence $[0/45/90/-45_2/90/45/0]_S$

The FLEXI-3 is composed of total 4 different groups (modules) of sandwich panels and any group can influence the lateral frequency. Thus any combination of skin thicknesses shall be applied to all panels. Using fairly simple rules of combinatorics, one can find a total of 81 possible configurations (4^3) that shall be analysed for eigenfrequencies.

To have an idea about the configurations in terms of skin thickness for each module, first few of them are listed in Table 3.2 . The complete list can be found in Appendix A.

¹Each laminate can be described by its own specific stiffness matrix which depends on elastic properties of the laminate's individual plies. The stiffness matrix is composed of three different submatrices, one of them being called membrane submatrix. The laminate is called 'quasi-isotropic' in case the membrane submatrix is isotropic, i.e. it shows identical elastic properties in all directions. [39]

Mass calculation

Next step is the assessment of weight penalty caused by the thickness variation for each configuration. Mass of the sandwich panel in particular configuration is calculated as

$$m_p = m_s + m_c = 2A_p t_s \rho_s + A_p (t_p - 2t_s) \rho_c \quad (3.1)$$

where m_s and m_c are the skin and the core masses, respectively, A_s is the surface area of the panel, t_s and t_p are the skin and the panel thicknesses, respectively, and ρ_s and ρ_c are the skin and the core densities.

Mass difference with respect to the default configuration is

$$\Delta m = m_p - m_d \quad (3.2)$$

where m_d is the mass of the panels in the default configuration, taken directly from a CAD model mass budget. A total delta mass (for all the panels) was evaluated for each configuration. First few are presented in Table 3.2 and the full list is again available in Appendix A.

Tab. 3.2: List of configurations

Config	Skin thickness [mm]				Delta mass [kg]
	HM	MD	TM	SWM	
CONFIG1	1	1	1	1	-8.34
CONFIG2	1	1	1	1.5	-3.13
CONFIG3	1	1	1	2	2.08
CONFIG4	1	1	1.5	1	1.27
CONFIG5	1	1	1.5	1.5	6.48
CONFIG6	1	1	1.5	2	11.69
CONFIG7	1	1	2	1	10.88
...
CONFIG81	2	2	2	2	49.56

FE model modification

After defining all the configurations and assessing their mass deviations from the default model, the optimization is only a matter of exporting all the combinations into solver decks and running the modal analyses for each of them. To ease the model export and to speed up the process, the default FE model was modified into *the optimization model*. What makes the optimization model different from the default one

is the way that the sandwich panel skins are modelled from material and properties point of view. In the optimization model, the skins are treated as isotropic components, rather than laminates, taking advantage of the quasi-isotropic behaviour which was discussed above. Equivalent modulus of elasticity, shear modulus and Poisson's ratio are determined by the membrane submatrix of the laminate.

The actual values of the equivalent laminate properties were extracted from custom MS Excel laminate solver and double-checked by the HyperLaminate².

$$E_{eq} = 124 \text{ GPa}$$

$$G_{eq} = 47 \text{ GPa}$$

$$\mu_{eq} = 0.31$$

To make the explanation above more clear, the main differences regarding modelling techniques for both models are shown in Table 3.3.

Tab. 3.3: Modelling techniques for composite components

	Model	
	Default	Optimization
Element topology	2D	2D
Nastran property	PCOMP	PSHELL
Nastran material	MAT8	MAT1
Elastic behaviour	Driven by stiffness matrix	Driven by equivalent moduli

With the model being modified as described, a modal analysis was run again with the optimization model, extracting all the eigenfrequencies up to 100 Hz. Main modes were found at 11.80 Hz and 54.28 Hz, showing that the model simplification is essentially correct and usable in terms of stiffness.

From the optimization model, solver decks (for all configurations) needed for the optimization can be exported by a simple skin thickness value change for each panel. In other words, this approach is more user friendly as far as model management goes.

Analyses

The last and the most important step of the optimization is running a modal analysis for each configuration, extracting the eigenfrequencies and evaluation of the main modes. A first configuration to exceed the natural frequency of 12 Hz in lateral direction while showing the least amount of delta mass is declared to be *the optimized structure*.

²Internal HyperMesh environment developed for modelling of composites.

3.2.2 Optimization results

After post-processing the results, CONFIG37 came out as the optimal solution in terms of both stiffness and weight penalty (see Appendix A for unfiltered results). A comparison with the default structure is herein provided:

Tab. 3.4: Optimization results

	Structure	
	Default	Optimized
First lateral frequency	11.82 Hz	12.04 Hz
First axial frequency	54.32 Hz	55.88 Hz
Structure mass	461.50 kg	467.30 kg
Weight penalty	-	5.80 kg
Weight penalty	-	1.26%
HM skin thickness	2 mm	1.5 mm
MD skin thickness	1 mm	1.5 mm
TM skin thickness	1 mm	1 mm
SWM skin thickness	1 mm	1 mm

As can be seen from Table 3.4, the stiffness limit regarding the natural frequency in lateral direction was reached with the listed configuration at the cost of additional 5.80 kg of structure mass. Also, the first axial frequency value was found being still safely above the desired limit (this was expected, since the main axial frequency for the default model is already high enough).

It is obvious from the optimized configuration that the changes are related only to the Hexagonal Module and the Main Deck panels. To have a little more insight into the structural behaviour regarding stiffness or mass in relation with thickness variation, see Figure 3.1 and Figure 3.2.

In Figure 3.1, each point represents a shift in first lateral frequency of the structure when the specific panel skin thickness is gradually being increased, while the other panels skins are fixed at 1 mm. Therefore the graph basically depicts how the different modules influence the overall FLEXI-3 stiffness. It needs to be emphasized that the dashed lines in the graph do not really illustrate a real course of the function between the points, as they are used only to make the graph more readable.

Similarly, Figure 3.2 represents how overall mass of the structure changes when the panels skins are modified separately. The mass difference is related to the structure in default configuration.

Even though the graphs do not cover the full set of configurations, it is already clear that the MD has by far the highest influence on the lateral frequency. The weight penalty it causes is, to some extent, balanced by the HM weight reduction, since its skins are already 2 mm thick in the default configuration and are reduced to 1.5 mm in the optimized variant.

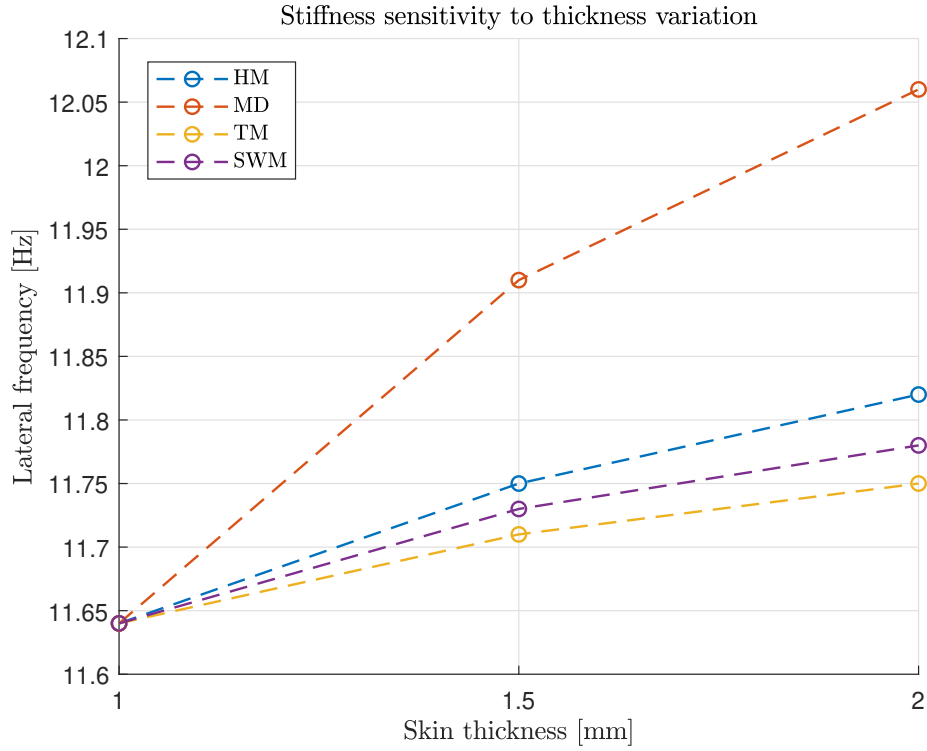


Fig. 3.1: Stiffness sensitivity to thickness variation

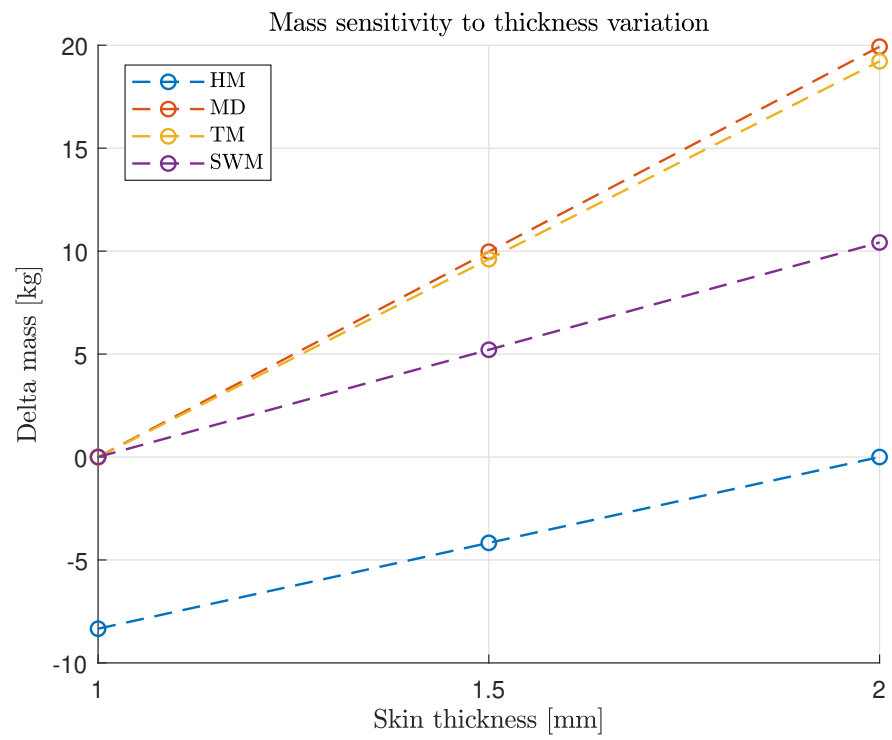


Fig. 3.2: Mass sensitivity to thickness variation

4 Strength verification

As it was highlighted before, the sandwich panels also serve as primary load paths for the structure. This short chapter provides at least basic strength verification of the most important components to prove that the optimized variant of the structure does not fail when subjected to launch related loads.

4.1 Design loads

The QSL for different flight phases introduced in 1.4.1 are considered as *limit loads* (LL). However, to determine *design limit loads* (DLL) for a space vehicle design process, additional factors shall be applied. Following a satellite design logic according to [40], the design limit loads are calculated as

$$DLL = C_A \cdot LL \quad (4.1)$$

where C_A is a design factor further determined by additional factors as

$$C_A = K_Q \cdot K_P \cdot K_M \quad (4.2)$$

where K_Q is the qualification factor representing loads modification for test campaign, K_P is the project factor taking into account the program maturity and design confidence and K_M is the model factor applied to account for uncertainties in mathematical models. [40] With $K_Q = 1.25$ (resulting from the satellite design logic [40]), $K_P = 1$ and $K_M = 1.2$ (agreed with ESA for the SSMS programme), the design factor has a final value of $C_A = 1.5$.

The DLL are then, according to Equation 4.1, reported in Table 4.1:

Tab. 4.1: DLL values for dimensioning of the FLEXI-3

Load event	QSL [g]		
	Longitudinal		Lateral
	Minimum	Maximum	
Lift-off	−6.75	+4.50	±2.03
Max. dynamic pressure	−6.45	+4.50	±1.35
1 st stage flight	−7.50	+1.50	±1.05
2 nd stage flight	−7.50	+4.50	±1.95
3 rd stage flight	−10.05	0.00	±0.30
AVUM+ flight	−1.50	+0.75	±1.05

Taking into account the fact that the lateral acceleration can act in any direction, a total of 156 load cases were derived from the listed QSL, covering 120° of the FLEXI-3 (taking advantage of symmetry). The load cases are all reported in a separate table within Appendix B.

4.2 Stress evaluation and margin philosophy

In a similar way the unit-gravity check from 2.5.2 was performed, the structural stress evaluation is done by standard SOL 101 run while implementing all the load cases from above into the solver deck and forcing Nastran to output von Mises stresses on isotropic components and failure indices on composites.

Last step before the final strength assessment is including relevant safety factors into the Nastran output. As it is defined in ECSS [40], safety factors used for the structural design shall be

$$SF_y = 1.10$$

$$SF_u = 1.25$$

where SF_y and SF_u are safety factors against yield and ultimate, respectively.

Margin of safety (MoS) for von Mises stress indicates the amount by which the allowable stress, defined by the material characteristics, exceeds the actual stress due to the applied loads, taking into account the applicable SF. It is calculated in the following manner

$$MoS = \frac{\sigma_S}{SF \cdot \sigma_{VM}} - 1 \quad (4.3)$$

where σ_S is yield or ultimate strength of the material, SF is the safety factor against yield or ultimate strength and σ_{VM} is calculated von Mises stress. The resulting MoS shall be positive ($MoS \geq 0$).

Failure index for composite components is according to Tsai-Hill failure criterion [41] defined as follows

$$FI = \frac{(SF_u \cdot \sigma_1)^2}{X^2} - \frac{SF_u \cdot \sigma_1 \cdot \sigma_2}{X^2} + \frac{(SF_u \cdot \sigma_2)^2}{Y^2} + \frac{(SF_u \cdot \tau_{12})^2}{S^2} \quad (4.4)$$

where σ_1 and σ_2 are calculated stresses along 0° and 90° direction, respectively, τ_{12} is calculated in-plane shear stress and X , Y and S are the material allowables in 0°, 90° and shear directions respectively (depending on the direction of σ_1 and σ_2 , the allowables X and Y are for tension or compression). As determined by the Tsai-Hill criterion, ply failure occurs when FI reaches 1. Thus the resulting FI shall be lower than 1 ($FI < 1$).

4.3 Strength verification results

4.3.1 Metallic components

Maximum von Mises stresses for aluminium machined parts evaluated throughout all the defined load cases are plotted in Figure 4.1.

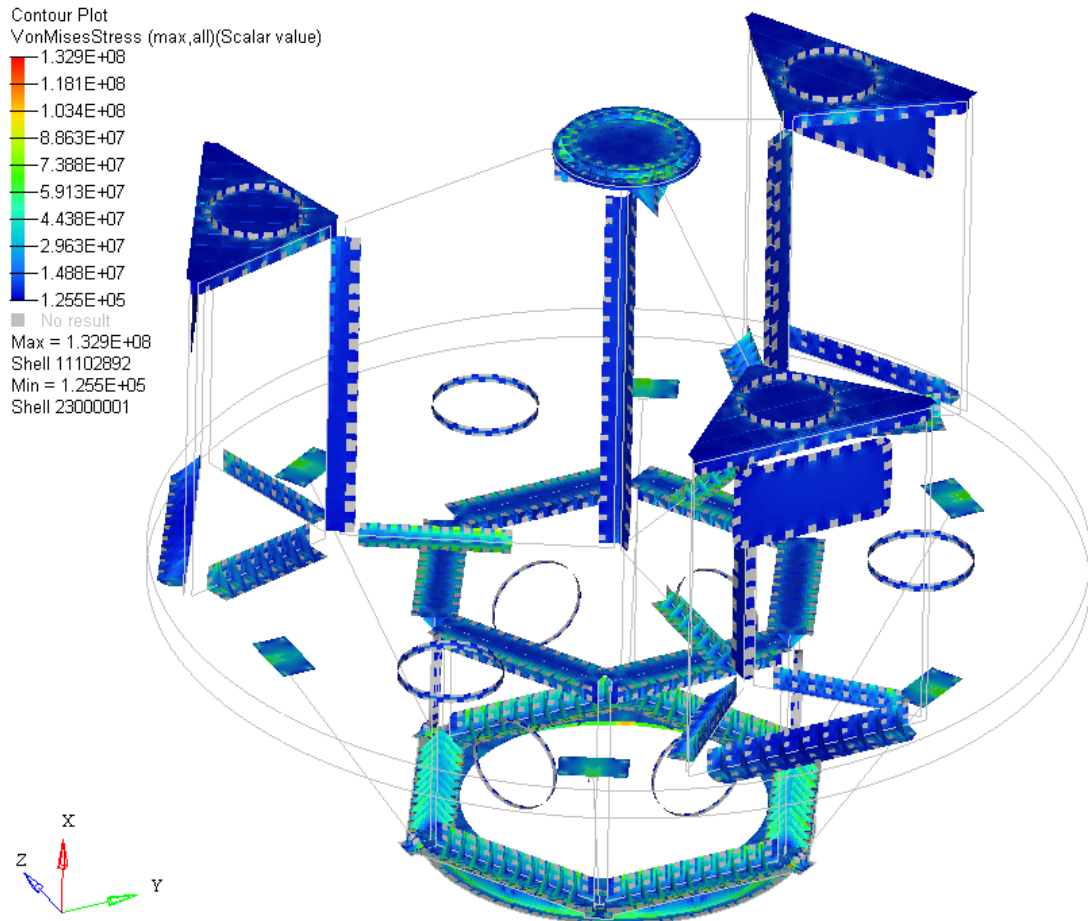


Fig. 4.1: Maximum von Mises stress for metallic components

Considering the safety factors for yield and ultimate strength, all MoS came out positive from the calculation.

4.3.2 Composite components

For sandwich panels skins and composite brackets, maximum failure indices evaluated throughout all the defined load cases are plotted in Figure 4.2. The safety factors from Equation 4.4 are not taken into account, as Nastran does not include them in the FI evaluation.

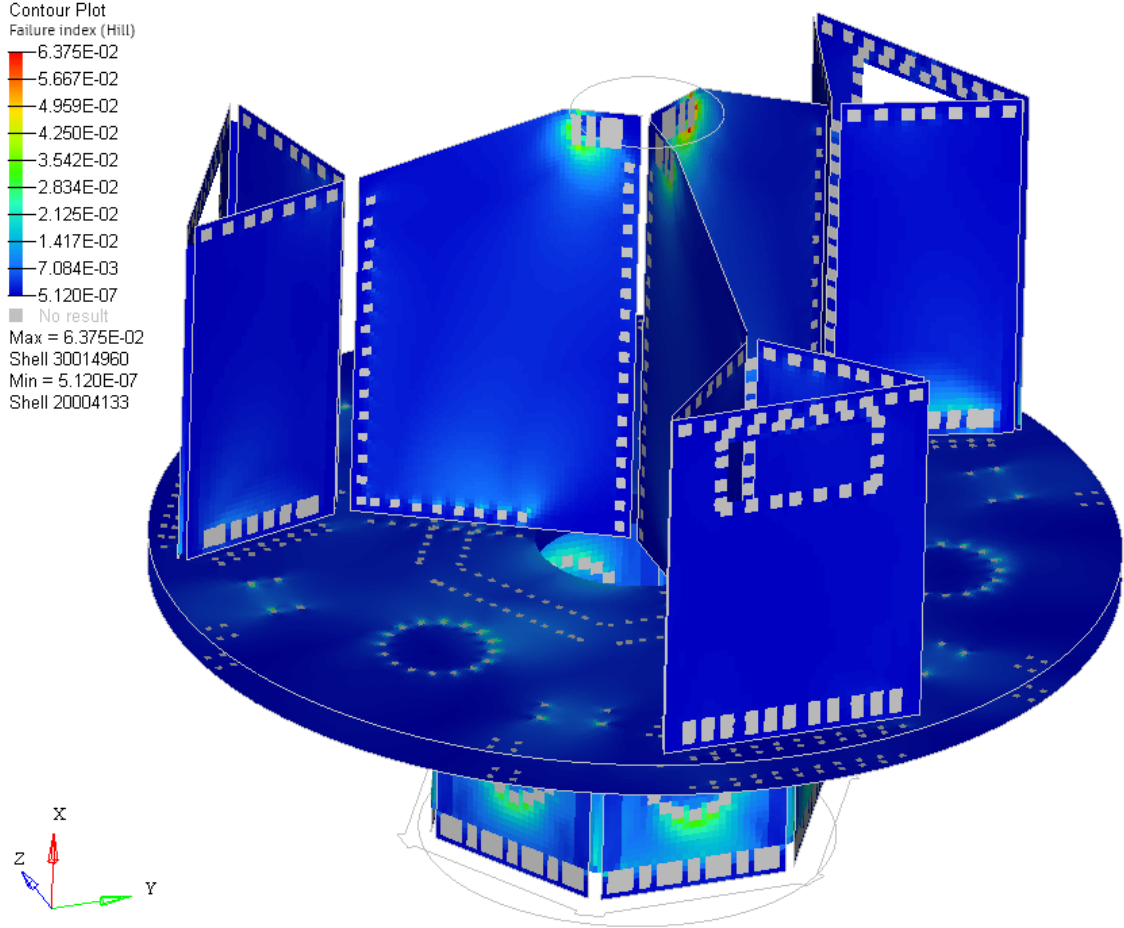


Fig. 4.2: Maximum failure index (Tsai-Hill) for composite components

When relevant safety factors are applied, the worst resulting failure index is $FI = 0.1$, meaning there is no ply failure in the structure for the L-QSL.

4.4 Conclusion and manufacturability analysis

Sections 4.3.1 and 4.3.2 have proven the structural resistance against the launch related loads even after the modifications related to performed optimization. This is the first step to successful structural dimensioning of the FLEXI-3. However, more analyses (fasteners, inserts, rivets, buckling, core failures, frequency response, etc.)

are to come, but they are beyond the thesis goals. Local resonances of the payloads found by future dynamic response analyses (sine, shock or random vibration) can reveal further load cases which can actually be more severe than the ones related to the launch. Thus a need to incorporate structural doublers¹ or core splices² may rise, which will eventually lead to further mass increase. This additional mass increase, however, is more related to potential strength issues (which would probably rise regardless of the optimization) than to the actual stiffness optimization performed in this thesis.

As far as manufacturability of the optimized variant is concerned, there is little to discuss. The technological aspects of the sandwich panels and the machined parts manufacturing process basically remain the same as they would be prior to the optimization, since the overall panel thickness remains unchanged and there is no interference with the rest of the structure, hence there is no need of modification. The sandwich panels will undergo ordinary autoclave curing cycle with adhesive bonding of the core, with only some of the skins having different number of pre-preg plies resulting from the optimization outcome.

¹An area on the surface of the panel where the skin is locally reinforced by additional pre-preg plies due to excessive loading of the structure caused by local resonances of the payloads.

²A local reinforcement of the honeycomb (e.g. usage of smaller cells or thicker cell sheets) due to local failures like core crushing or core buckling.

Conclusion

This thesis started by a summary of European space activities and along with launchers technical overview, it provided necessary introduction and background for the later chapters.

Complex engineering problems like the required structural optimization of the SSMS Dispenser are almost exclusively tied to the computational modelling. As the Dispenser is a very large and complex structure, a standalone chapter was dedicated to the finite element model development. This chapter showed difficulties of the modelling and highlighted the fact that the computational models shall always undergo proper mathematical validation process before the results are declared as reliable.

Modal analysis of the Dispenser revealed the main lateral mode being at 11.82 Hz, proving that the current design did not comply with the stiffness requirement for lateral direction. The main axial mode was found beyond required 50 Hz. Several optimization methods were proposed with emphasis put on expressing pros and cons for each method. The optimization was performed by chosen and justified method and its results were clearly identified as follows: the influence of the upper modules (TM and SWM) on the eigenfrequencies is rather minor and most of the stiffness is provided by the MD, where the skin thickness is proposed to increase from 1 mm to 1.5 mm. At the same time, the HM sandwich panels came out of the optimization overdimensioned in terms of stiffness, making it possible to propose skin thickness reduction from 2 mm to 1.5 mm. This change, to some extent, balances the quite significant weight penalty caused by the MD reinforcement. Resulting weight penalty of 5.80 kg is the very minimum that was possible to achieve by the proposed method of optimization. The first lateral frequency for the modified variant was found at 12.04 Hz. Along with the first axial frequency being 55.88 Hz, it can be stated that the stiffness criteria were met.

An effort to achieve compliance with the eigenfrequency limits can compromise strength and vice versa. Proposed changes on the HM skin prove that stiffness and strength of the structure act against each other in this case. That is why the strength verification was performed in the end for the most important structural components. A total of 156 load cases were investigated and all resulted into positive margins of safety. Even though there are more detailed analyses to come in finalization phase of the design, the performed verification implies that the structure is resistant to the launch related loads even after the design modifications.

Bibliography

- [1] *ESA - A European vision* [online] [cit. 2020-03-26]. Available at: http://www.esa.int/About_Us/Corporate_news/A_European_vision
- [2] *European Space Agency: Facts and Information* [online] [cit. 2020-03-26]. Available at: <https://www.space.com/22562-european-space-agency.html>
- [3] *ESA - ESA's Purpose* [online] [cit. 2020-03-26]. Available at: http://www.esa.int/About_Us/Corporate_news/ESA_s_Purpose
- [4] *ESA - ESA and the EU* [online] [cit. 2020-03-26]. Available at: http://www.esa.int/About_Us/Corporate_news/ESA_and_the_EU
- [5] *ESA - Member States and Cooperating States* [online] [cit. 2020-03-27]. Available at: https://www.esa.int/About_Us/Corporate_news/Member_States_Cooperating_States
- [6] *ESA - ESA facts* [online] [cit. 2020-03-27]. Available at: http://www.esa.int/About_Us/Corporate_news/ESA_facts
- [7] *ESA - Funding* [online] [cit. 2020-03-27]. Available at: https://www.esa.int/About_Us/Corporate_news/Funding
- [8] *ESA - Our Missions* [online] [cit. 2020-03-28]. Available at: https://www.esa.int/ESA/Our_Missions
- [9] *ESA - Copernicus overview* [online] [cit. 2020-03-28]. Available at: https://www.esa.int/Applications/Observing_the_Earth/Copernicus/Overview3
- [10] *ESA - What is Galileo?* [online] [cit. 2020-03-28]. Available at: https://www.esa.int/Applications/Navigation/Galileo/What_is_Galileo
- [11] *ESA - Space Transportation strategy* [online] [cit. 2020-03-29]. Available at: https://www.esa.int/Enabling_Support/Space_Transportation/Space_Transportation_strategy
- [12] *ESA - Space Transportation and industry* [online] [cit. 2020-03-29]. Available at: http://www.esa.int/Enabling_Support/Space_Transportation/Space_Transportation_and_industry
- [13] *ESA - EDU esa exp* [online] [cit. 2020-03-29]. Available at: https://www.esa.int/ESA_Multimedia/Images/2009/07/EDU_esa_exp_-_Launchers

- [14] *ESA - Vega* [online] [cit. 2020-03-30]. Available at: https://www.esa.int/Enabling_Support/Space_Transportation/Launch_vehicles/Vega
- [15] *ESA - Ariane 5 ECA* [online] [cit. 2020-03-30]. Available at: http://www.esa.int/Enabling_Support/Space_Transportation/Launch_vehicles/Ariane_5_ECA2
- [16] *ESA - Soyuz* [online] [cit. 2020-03-30]. Available at: https://www.esa.int/Enabling_Support/Space_Transportation/Launch_vehicles/Soyuz
- [17] *ESA - Vega-C* [online] [cit. 2020-03-30]. Available at: https://www.esa.int/Enabling_Support/Space_Transportation/Launch_vehicles/Vega-C
- [18] *ESA - Ariane 6* [online] [cit. 2020-03-30]. Available at: https://www.esa.int/Enabling_Support/Space_Transportation/Launch_vehicles/Ariane_6
- [19] *Vega C User's Manual* [online] Issue 0 Revision 0. 2018 [cit. 2020-04-03]. Available at: https://www.arianespace.com/wp-content/uploads/2018/07/Vega-C-user-manual-Issue-0-Revision-0_20180705.pdf
- [20] *Vega User's Manual* [online] Issue 4 Revision 0. 2014 [cit. 2020-04-03]. Available at: https://www.arianespace.com/wp-content/uploads/2015/09/Vega-Users-Manual_Issue-04_April-2014.pdf
- [21] *ESA - Vega-C fairing's trial by sound* [online] [cit. 2020-04-03]. Available at: https://www.esa.int/ESA_Multimedia/Images/2019/11/Vega-C_fairing_s_trial_by_sound
- [22] *ESA - Vega flight opportunity for multiple small satellites* [online] [cit. 2020-04-08]. Available at: https://www.esa.int/Enabling_Support/Space_Transportation/Vega_flight_opportunity_for_multiple_small_satellite
- [23] CARAMELLI, Fabio. *The first Vega ride-share mission flight*. [online]. [cit. 2020-04-08]. Available at: <https://digitalcommons.usu.edu/cgi/viewcontent.cgi?article=4444&context=smallsat>
- [24] *ESA - SSMS vibration testing* [online] [cit. 2020-04-09]. Available at: https://www.esa.int/ESA_Multimedia/Images/2019/06/SSMS_vibration_testing
- [25] MACDONALD, Malcolm a Viorel BADESCU, ed. *The international handbook of space technology*. Berlin: Springer, c2014. ISBN 978-3-642-41100-7.
- [26] *VECEP Program SSMS Dispenser Functional Requirement Specification* Issue 2. 2017

- [27] WIJKER, J. J. *Spacecraft structures*. Berlin: Springer, 2008. ISBN 978-3-540-75552-4.
- [28] *HexWeb® Honeycomb Selector Guide* [online] [cit. 2020-05-17]. Available at: https://www.hexcel.com/user_area/content_media/raw/HexWeb_SelectorGuide_2017.pdf
- [29] *MAT9 / Nastran 2019 / Autodesk Knowledge Network* [online] [cit. 2020-05-17]. Available at: <https://knowledge.autodesk.com/support/nastran/learn-explore/caas/CloudHelp/cloudhelp/2019/ENU/NSTRN-Reference/files/GUID-8696A4EA-0499-40B9-BF4F-F3E0446331CC-htm.html>
- [30] *2000785F MkII MLB User Manual* [online] Rev D. Planetary Systems Corporation, 2014 [cit. 2020-04-23]. Available at: <http://www.planetarysystemscorp.com/wp-content/uploads/2015/08/2000785F-MkII-MLB-User-Manual.pdf>
- [31] *FEMCI Book* [online] [cit. 2020-04-22]. Available at: <https://femci.gsfc.nasa.gov/validitychecks/index.html>
- [32] *FEMCI Book - Unit Gravity Loading Validity Check* [online] [cit. 2020-04-16]. Available at: <https://femci.gsfc.nasa.gov/validitychecks/vc3.html>
- [33] ECSS-E-ST-32-03C. *Space engineering: Structural finite element models*. Noordwijk (The Netherlands): ESA Requirements and Standards Division, 2008.
- [34] *FEMCI Book - Free-Free Dynamics Validity Check* [online] [cit. 2020-04-15]. Available at: <https://femci.gsfc.nasa.gov/validitychecks/vc2.html>
- [35] *Basic Dynamic Analysis User's Guide* [online]. Siemens Product Lifecycle Management Software Inc., 2014 [cit. 2020-04-23]. Available at: https://docs.plm.automation.siemens.com/data_services/resources/nxnastran/10/help/en_US/tdocExt/pdf/basic_dynamics.pdf
- [36] FISH, Jacob and Ted BELYTSCHKO. *A First Course in Finite Elements*. Chichester: Wiley, 2007. ISBN 978-0-470-03580-1.
- [37] *HexWeb™ Honeycomb Sandwich Design Technology* [online] [cit. 2020-06-11]. Available at: https://www.hexcel.com/user_area/content_media/raw/Honeycomb_Sandwich_Design_Technology.pdf
- [38] PLANTEMA, Frederik J. *Sandwich Construction: The Bending and Buckling of Sandwich Beams, Plates and Shells*. 1st Edition, New York: John Wiley and Sons, 1966. ISBN 978-0471691068.

- [39] JURAČKA, Jaroslav. *Kompozitní konstrukce v letectví*. Rev. 9. Letecký ústav, VUT v Brně, 2017.
- [40] ECSS-E-ST-32-10C. *Space engineering: Structural factors of safety for space-flight hardware*. Rev. 1. Noordwijk (The Netherlands): ESA Requirements and Standards Division, 2009.
- [41] NIU, Michael. *Composite Airframe Structures*. Hong Kong Conmilit Press Ltd., 2010. ISBN 9789627128069.

List of abbreviations and symbols

AVUM	Attitude and Vernier Upper Module
CAD	Computer Aided Design
CFRP	Carbon Fibre Reinforced Polymer
CoG	Centre of Gravity
CS	Coordinate System
DLL	Design Limit Load
ECSS	European Cooperation for Space Standardization
ELDO	European Launcher Development Organisation
ESA	European Space Agency
ESRO	European Space Research Organisation
ESTEC	European Space Research and Technology Centre
EU	European Union
FE	Finite Element
FI	Failure Index
GPS	Global Positioning System
GTO	Geostationary Transfer Orbit
HM	Hexagonal Module
LB	Lightband
LC	Load Case
LL	Limit Load
LLL	Light satellite, Low-cost Launch
MD	Main Deck
MEO	Medium Earth Orbit
MoS	Margin of Safety
MPC	Multi-Point Constraint
NASA	National Aeronautics and Space Administration
P/L	Payload
PoC	Proof of Concept
QSL	Quasi-Static Load
SF	Safety Factor
SI	International System of Metric Units
SPC	Single-Point Constraint
SRS	Shock Response Spectrum
SSMS	Small Spacecraft Mission Service
SSO	Sun Synchronous Orbit
SWM	Shear Web Module
TM	Tower Module

\mathbf{A}	eigenvector
A_p	surface area of the panel
C_A	design factor
E	Young's modulus (isotropic material)
E_{eq}	equivalent modulus of elasticity (quasi-isotropic laminate)
E_1	tensile modulus for fibre direction (orthotropic material)
E_2	tensile modulus for matrix direction (orthotropic material)
f_{lat}	lateral frequency
f_{ax}	longitudinal frequency
\mathbf{F}	vector of nodal external loads
g	gravitational acceleration
G_{eq}	equivalent shear modulus (quasi-isotropic laminate)
G_{12}	in-plane shear modulus (orthotropic material)
G_{33}	compressive modulus (orthotropic material)
G_{55}	shear modulus (W-direction) (anisotropic material)
G_{66}	shear modulus (L-direction) (anisotropic material)
\mathbf{K}	stiffness matrix
K_M	model factor
K_P	project factor
K_Q	qualification factor
m_c	mass of the core
m_d	mass of the panel in default configuration
m_p	mass of the panel
m_s	mass of the skin
\mathbf{M}	mass matrix
S	material allowable for in-plane shear
SF_u	safety factor against ultimate strength
SF_y	safety factor against yield strength
t	time
t_s	skin thickness
\mathbf{u}	vector of nodal displacements
X	material allowable in 0° direction
Y	material allowable in 90° direction
δF	residual force
δW	residual work
Δm	mass difference
ε	ratio of residual work

μ	Poisson's ratio (isotropic material)
μ_{eq}	equivalent Poisson's ratio (quasi-isotropic laminate)
μ_{12}	in-plane Poisson's ratio (orthotropic material)
ρ_c	core material density
ρ_s	skin material density
σ_S	strength of the material (yield or ultimate)
σ_{VM}	von Mises stress
σ_1	calculated normal stress along 0° direction
σ_2	calculated normal stress along 90° direction
τ_{12}	calculated in-plane shear stress
ω^2	eigenvalue

List of appendices

A Optimization results	73
B Load cases	76

A Optimization results

Config	Skin thickness [mm]				Mass and frequency	
	HM	MD	TM	SWM	Delta [kg]	Lateral [Hz]
CONFIG1	1	1	1	1	-8.34	11.64
CONFIG2	1	1	1	1.5	-3.13	11.73
CONFIG3	1	1	1	2	2.08	11.78
CONFIG4	1	1	1.5	1	1.27	11.71
CONFIG5	1	1	1.5	1.5	6.48	11.80
CONFIG6	1	1	1.5	2	11.69	11.85
CONFIG7	1	1	2	1	10.88	11.75
CONFIG8	1	1	2	1.5	16.09	11.84
CONFIG9	1	1	2	2	21.29	11.89
CONFIG10	1	1.5	1	1	1.63	11.91
CONFIG11	1	1.5	1	1.5	6.84	11.99
CONFIG12	1	1.5	1	2	12.04	12.05
CONFIG13	1	1.5	1.5	1	11.24	11.97
CONFIG14	1	1.5	1.5	1.5	16.44	12.06
CONFIG15	1	1.5	1.5	2	21.65	12.11
CONFIG16	1	1.5	2	1	20.84	12.00
CONFIG17	1	1.5	2	1.5	26.05	12.09
CONFIG18	1	1.5	2	2	31.26	12.14
CONFIG19	1	2	1	1	11.59	12.06
CONFIG20	1	2	1	1.5	16.80	12.16
CONFIG21	1	2	1	2	22.01	12.21
CONFIG22	1	2	1.5	1	21.20	12.12
CONFIG23	1	2	1.5	1.5	26.41	12.22
CONFIG24	1	2	1.5	2	31.62	12.27
CONFIG25	1	2	2	1	30.81	12.14
CONFIG26	1	2	2	1.5	36.02	12.25
CONFIG27	1	2	2	2	41.22	12.30
CONFIG28	1.5	1	1	1	-4.17	11.75
CONFIG29	1.5	1	1	1.5	1.04	11.84
CONFIG30	1.5	1	1	2	6.25	11.89
CONFIG31	1.5	1	1.5	1	5.44	11.83
CONFIG32	1.5	1	1.5	1.5	10.65	11.92
CONFIG33	1.5	1	1.5	2	15.85	11.97
CONFIG34	1.5	1	2	1	15.05	11.87

Config	Skin thickness [mm]				Mass and frequency	
	HM	MD	TM	SWM	Delta [kg]	Lateral [Hz]
CONFIG35	1.5	1	2	1.5	20.25	11.96
CONFIG36	1.5	1	2	2	25.46	12.01
CONFIG37	1.5	1.5	1	1	5.80	12.04
CONFIG38	1.5	1.5	1	1.5	11.00	12.13
CONFIG39	1.5	1.5	1	2	16.21	12.18
CONFIG40	1.5	1.5	1.5	1	15.40	12.10
CONFIG41	1.5	1.5	1.5	1.5	20.61	12.20
CONFIG42	1.5	1.5	1.5	2	25.82	12.26
CONFIG43	1.5	1.5	2	1	25.01	12.13
CONFIG44	1.5	1.5	2	1.5	30.22	12.24
CONFIG45	1.5	1.5	2	2	35.43	12.29
CONFIG46	1.5	2	1	1	15.76	12.20
CONFIG47	1.5	2	1	1.5	20.97	12.30
CONFIG48	1.5	2	1	2	26.18	12.36
CONFIG49	1.5	2	1.5	1	25.37	12.26
CONFIG50	1.5	2	1.5	1.5	30.58	12.37
CONFIG51	1.5	2	1.5	2	35.79	12.42
CONFIG52	1.5	2	2	1	34.98	12.29
CONFIG53	1.5	2	2	1.5	40.19	12.40
CONFIG54	1.5	2	2	2	45.39	12.46
CONFIG55	2	1	1	1	0.00	11.82
CONFIG56	2	1	1	1.5	5.21	11.91
CONFIG57	2	1	1	2	10.42	11.96
CONFIG58	2	1	1.5	1	9.61	11.90
CONFIG59	2	1	1.5	1.5	14.82	11.99
CONFIG60	2	1	1.5	2	20.02	12.05
CONFIG61	2	1	2	1	19.22	11.94
CONFIG62	2	1	2	1.5	24.42	12.03
CONFIG63	2	1	2	2	29.63	12.09
CONFIG64	2	1.5	1	1	9.97	12.11
CONFIG65	2	1.5	1	1.5	15.17	12.21
CONFIG66	2	1.5	1	2	20.38	12.26
CONFIG67	2	1.5	1.5	1	19.57	12.18
CONFIG68	2	1.5	1.5	1.5	24.78	12.28
CONFIG69	2	1.5	1.5	2	29.99	12.36
CONFIG70	2	1.5	2	1	29.18	12.21

Config	Skin thickness [mm]				Mass and frequency	
	HM	MD	TM	SWM	Delta [kg]	Lateral [Hz]
CONFIG71	2	1.5	2	1.5	34.39	12.32
CONFIG72	2	1.5	2	2	39.60	12.37
CONFIG73	2	2	1	1	19.93	12.28
CONFIG74	2	2	1	1.5	25.14	12.38
CONFIG75	2	2	1	2	30.35	12.44
CONFIG76	2	2	1.5	1	29.54	12.34
CONFIG77	2	2	1.5	1.5	34.75	12.45
CONFIG78	2	2	1.5	2	39.96	12.51
CONFIG79	2	2	2	1	39.15	12.37
CONFIG80	2	2	2	1.5	44.35	12.48
CONFIG81	2	2	2	2	49.56	12.54

B Load cases

Lift-off phase							
LC	Acceleration [g]			LC	Acceleration [g]		
	x	y	z		x	y	z
1	-6.75	0.00	2.03	14	4.50	0.00	2.03
2	-6.75	0.35	1.99	15	4.50	0.35	1.99
3	-6.75	0.69	1.90	16	4.50	0.69	1.90
4	-6.75	1.01	1.75	17	4.50	1.01	1.75
5	-6.75	1.30	1.55	18	4.50	1.30	1.55
6	-6.75	1.55	1.30	19	4.50	1.55	1.30
7	-6.75	1.75	1.01	20	4.50	1.75	1.01
8	-6.75	1.90	0.69	21	4.50	1.90	0.69
9	-6.75	1.99	0.35	22	4.50	1.99	0.35
10	-6.75	2.03	0.00	23	4.50	2.03	0.00
11	-6.75	1.99	-0.35	24	4.50	1.99	-0.35
12	-6.75	1.90	-0.69	25	4.50	1.90	-0.69
13	-6.75	1.75	-1.01	26	4.50	1.75	-1.01
Max. dynamic pressure phase							
LC	Acceleration [g]			LC	Acceleration [g]		
	x	y	z		x	y	z
27	-6.45	0.00	1.35	40	4.50	0.00	0.00
28	-6.45	0.23	1.33	41	4.50	0.00	0.00
29	-6.45	0.46	1.27	42	4.50	0.00	0.00
30	-6.45	0.68	1.17	43	4.50	0.00	0.00
31	-6.45	0.87	1.03	44	4.50	0.00	0.00
32	-6.45	1.03	0.87	45	4.50	0.00	0.00
33	-6.45	1.17	0.68	46	4.50	0.00	0.00
34	-6.45	1.27	0.46	47	4.50	0.00	0.00
35	-6.45	1.33	0.23	48	4.50	0.00	0.00
36	-6.45	1.35	0.00	49	4.50	0.00	0.00
37	-6.45	1.33	-0.23	50	4.50	0.00	0.00
38	-6.45	1.27	-0.46	51	4.50	0.00	0.00
39	-6.45	1.17	-0.68	52	4.50	0.00	0.00

1st stage flight phase							
LC	Acceleration [g]			LC	Acceleration [g]		
	x	y	z		x	y	z
53	-7.50	0.00	1.05	66	1.50	0.00	1.05
54	-7.50	0.18	1.03	67	1.50	0.18	1.03
55	-7.50	0.36	0.99	68	1.50	0.36	0.99
56	-7.50	0.53	0.91	69	1.50	0.53	0.91
57	-7.50	0.67	0.80	70	1.50	0.67	0.80
58	-7.50	0.80	0.67	71	1.50	0.80	0.67
59	-7.50	0.91	0.53	72	1.50	0.91	0.53
60	-7.50	0.99	0.36	73	1.50	0.99	0.36
61	-7.50	1.03	0.18	74	1.50	1.03	0.18
62	-7.50	1.05	0.00	75	1.50	1.05	0.00
63	-7.50	1.03	-0.18	76	1.50	1.03	-0.18
64	-7.50	0.99	-0.36	77	1.50	0.99	-0.36
65	-7.50	0.91	-0.53	78	1.50	0.91	-0.53
2nd stage flight phase							
LC	Acceleration [g]			LC	Acceleration [g]		
	x	y	z		x	y	z
79	-7.50	0.00	1.95	92	4.50	0.00	1.95
80	-7.50	0.34	1.92	93	4.50	0.34	1.92
81	-7.50	0.67	1.83	94	4.50	0.67	1.83
82	-7.50	0.98	1.69	95	4.50	0.98	1.69
83	-7.50	1.25	1.49	96	4.50	1.25	1.49
84	-7.50	1.49	1.25	97	4.50	1.49	1.25
85	-7.50	1.69	0.98	98	4.50	1.69	0.98
86	-7.50	1.83	0.67	99	4.50	1.83	0.67
87	-7.50	1.92	0.34	100	4.50	1.92	0.34
88	-7.50	1.95	0.00	101	4.50	1.95	0.00
89	-7.50	1.92	-0.34	102	4.50	1.92	-0.34
90	-7.50	1.83	-0.67	103	4.50	1.83	-0.67
91	-7.50	1.69	-0.98	104	4.50	1.69	-0.98

3rd stage flight phase							
LC	Acceleration [g]			LC	Acceleration [g]		
	x	y	z		x	y	z
105	-10.05	0.00	0.30	118	0.00	0.00	0.30
106	-10.05	0.05	0.30	119	0.00	0.05	0.30
107	-10.05	0.10	0.28	120	0.00	0.10	0.28
108	-10.05	0.15	0.26	121	0.00	0.15	0.26
109	-10.05	0.19	0.23	122	0.00	0.19	0.23
110	-10.05	0.23	0.19	123	0.00	0.23	0.19
111	-10.05	0.26	0.15	124	0.00	0.26	0.15
112	-10.05	0.28	0.10	125	0.00	0.28	0.10
113	-10.05	0.30	0.05	126	0.00	0.30	0.05
114	-10.05	0.30	0.00	127	0.00	0.30	0.00
115	-10.05	0.30	-0.05	128	0.00	0.30	-0.05
116	-10.05	0.28	-0.10	129	0.00	0.28	-0.10
117	-10.05	0.26	-0.15	130	0.00	0.26	-0.15
AVUM+ flight phase							
LC	Acceleration [g]			LC	Acceleration [g]		
	x	y	z		x	y	z
131	-1.50	0.00	1.05	144	0.75	0.00	1.05
132	-1.50	0.18	1.03	145	0.75	0.18	1.03
133	-1.50	0.36	0.99	146	0.75	0.36	0.99
134	-1.50	0.53	0.91	147	0.75	0.53	0.91
135	-1.50	0.67	0.80	148	0.75	0.67	0.80
136	-1.50	0.80	0.67	149	0.75	0.80	0.67
137	-1.50	0.91	0.53	150	0.75	0.91	0.53
138	-1.50	0.99	0.36	151	0.75	0.99	0.36
139	-1.50	1.03	0.18	152	0.75	1.03	0.18
140	-1.50	1.05	0.00	153	0.75	1.05	0.00
141	-1.50	1.03	-0.18	154	0.75	1.03	-0.18
142	-1.50	0.99	-0.36	155	0.75	0.99	-0.36
143	-1.50	0.91	-0.53	156	0.75	0.91	-0.53